Final Technical Report

Project Title:	Aging of Graphitic Cast Irons and Machinability
DOE Award Number:	DE-FC36-04GO14230
Project Period:	January 1, 2004 to June 30, 2012
Recipient Organization:	University of Missouri - Rolla
Technical Contact:	Von L. Richards
	Materials Science and Engineering Department
	Missouri University of Science and Technology
	1870 Miner Circle
	Rolla, MO 65409
	Telephone: 573-341-4730
	Fax: 573-341-6964
	Email: vonlr@mst.edu

Other Team Member Organizations: American Foundry Society, TKA Waupaca, Metals Technology, Inc., Dalton Foundry, ASAMA Coldwater Manufacturing, Motor Castings, MOOG Automotive, Wells Manufacturing

Date of report:	September 19, 2012

Acknowledgment: This report is based upon work supported by the U. S. Department of Energy under Award No DE-FC36-4GO14230.

Disclaimer: Any findings, opinions, and conclusions or recommendations expressed in this report are those of the author(s) and do not necessarily reflect the views of the Department of Energy.

Proprietary Data Notice: No proprietary data is contained within the report.

DOCUMENT AVAILABILITY

Reports produced after January 1, 1996, are available free via the U.S. Department of Energy (DOE) Information Bridge.

Web site http://www.osti.gov/bridge

Reports are available to DOE employees, DOE contractors, Energy Technology Data Exchange (ETDE) representatives, and International Nuclear Information System (INIS) representatives from the following source.

Office of Scientific and Technical Information
P.O. Box 62
Oak Ridge, TN 37831
Telephone 865-576-8401
Fax 865-576-5728
E-mail reports@osti.gov
Web site http://www.osti.gov/contact.html

This report was prepared as an account of work sponsored by an agency of the United States Government. Neither the United States Government nor any agency thereof, nor any of their employees, makes any warranty, express or implied, or assumes any legal liability or responsibility for the accuracy, completeness, or usefulness of any information, apparatus, product, or process disclosed, or represents that its use would not infringe privately owned rights. Reference herein to any specific commercial product, process, or service by trade name, trademark, manufacturer, or otherwise, does not necessarily constitute or imply its endorsement, recommendation, or favoring by the United States Government or any agency thereof. The views and opinions of authors expressed herein do not necessarily state or reflect those of the United States Government or any agency thereof.

ii

TABLE OF CONTENTS

List of Figures

iv

List of Tables

1. Executive Summary

This project addressed items under both of the stated metals casting challenges.

Design of Castings for New Markets: In strength limited applications of gray, ductile and compacted graphite (CG) iron, the results of this work will lead to reduced section sizes, and corresponding weight savings. Improved machinability will enhance casting marketability.

Improved Metal Casting Processes: This research will also lead to yield improvements by allowing the adjustment of casting compositions to higher CG compositions while meeting the same strength specification, but allowing casting with less gating and/or higher yield. The use of higher CG compositions will reduce scrap due to shrink and use of aging will reduce machinability rejects.

Nicola and Richards (1999) had demonstrated that age strengthening occurs in gray cast iron. Edington, Nicola and Richards (2002) had shown that the machinability of cast iron improves with age strengthening, and had shown evidence of a 0.2-0.4 nm precipitate formation by neutron scattering. The influence of nitrogen (Richards, Van Aken and Nicola, 2002) also suggested a nitrogen-containing precipitate. Considering the body of work in gray iron, it is important to study the extension of this process to the family of cast irons. Ductile iron and compacted graphite iron are particularly important product areas, since both offer the possibility of significant market growth and enhancement of energy savings from the application of the aging behavior to processes and design.

While the aging phenomenon has been demonstrated in gray cast iron, it needs to be studied in other graphitic cast iron alloys that are growing in application: ductile iron and compacted graphite iron. Initial studies have indicated that quench-and-temper processed ductile irons do not exhibit aging, which is consistent with the work of Nicola and Richards on accelerating the aging process. Some as-cast grades of ductile iron do show age strengthening; however this was not found to be true in ductile or CG iron produced by the Fischer Converter Process due to the low nitrogen resulting from the effect of the violent Magnesium (Mg) gas flush in the converter process. Compacted graphite iron is another alloy system in graphitic cast irons that has found extensive application recently. It was determined that the "denodulizing"' additions used in the wire feed process essentially combine with the nitrogen as well, causing it to be unavailable to participate in the age strengthening process. The only CG irons studied were made from this process and the fisher converter process; so we concluded that in general age strengthening is not observed to a significant extent in CG irons just due to the low soluble nitrogen.

The mechanism by which the machinability of cast iron improves with age strengthening was identified and demonstrated. Under this program, tool dynamometer measurements were used along with high speed video and statistical microscopy of machined chips to help characterize the changes of tool force due to aging. In addition, in-plant machinability studies were used to understand if the effects were industrially significant and to engage industrial sites as early adopters. Laboratory machinability studies were performed on ductile iron to see if age strengthening produces a corresponding change in machinability and whether the machinability improves as it does in gray iron. These

1

results showed that at high free ferrite content and nitrogen, in excess of stoichiometry with titanium, the machinability effects in ductile iron were significant. The machinability effect was again shown to depend on free ferrite content. The tool dynamometer with a data acquisition system and high speed video on a common timing trigger clearly explained the chip breaking and tool loading reduction effects of aging. Also, it became clear that there were metallurgical conditions necessary for age strengthening to improve machinability. When no free ferrite was present, the machinability decreases as the strength and hardness increases. In these cases the increase in hardness of the metal was not compensated by improved chip morphology.

The mechanism by which the nitrogen is involved in the age strengthening process in cast irons was significantly clarified. It had been speculated that there is nano-sized precipitation in the ferrite portion of the matrix structure. There was evidence from neutron scattering that 0.2-0.4 nm precipitates occur during room temperature aging. Differential scanning calorimetry work indicated that an iron carbo-nitride precipitation is a likely mechanism. Mechanical measurements such as strain hardening were also used as measurements to help with understanding the mechanism for the age strengthening.

Some work on the kinetics in gray iron has already been done. Careful study of the kinetics of age strengthening clarified the activation energy, growth morphologies of precipitates and the effects of trace elements and minor alloying elements such as Manganese (Mn) and Sulfur (S) on the rate. Acceleration of the aging process is critical to good business practices such as just-in-time manufacturing and Kanban inventory control. Also this would be a source of energy savings. As a final step an article was prepared for the American Foundry Society (AFS) on using thermal and alloy factors to maximize the rate.

Estimated energy savings in ten years was 13.05 trillion BTU, based primarily on yield improvement and size reduction of castings for equivalent service. Also it is estimated that the heavy truck end use of lighter castings for equivalent service requirement will result in a diesel fuel energy savings of 131 trillion BTU in ten years.

2. Introduction and Background

2.1.   Literature and Review

2.1.1. Machinability Definition and Quantification.

Machinability is defined as the ease with which a material can be machined into satisfactory parts.[1,2] In practice machinability is a complex property and no quantification or measurement method for machinability is universally accepted. Machinability has commonly been quantified by tool life or wear, machined surface finish, tool forces, characteristics of chips, power consumption during machining, metal removal rate, or a combination of these measurements. The International Standards Organization 3685-1993 standard attempts to standardize machinability through tool wear measurements at varied cutting speeds.[3] The American Foundry Society has established a standardized casting for tool life testing in an effort to make more comparable machinability results.[4]

2.1.2. Chip Formation.

When a material is machined, the portions of the workpiece removed are referred to as chips. Perhaps the most referenced publication into the nature of chip formation was by Hans Ernst.[5] His chip formation model became the basis for much future chip formation and morphology research and can be found in most textbooks that cover metal machining. Ernst described three basic chip types which are shown in Figure 1. The chips were determined to begin forming and complete most of their formation in an area called the shear zone. The shear zone is narrow enough that it is commonly approximated as a plane, dubbed the shear plane, which is at an angle to the workpiece called the shear angle. A schematic of the shear zone, shear plane, and shear angle is shown in Figure 2. An increase in shear angle will lower forces acting on the tool, thereby decreasing temperature at the tool/chip interface and reducing chip length.[6]

(1)   (2)   (3)
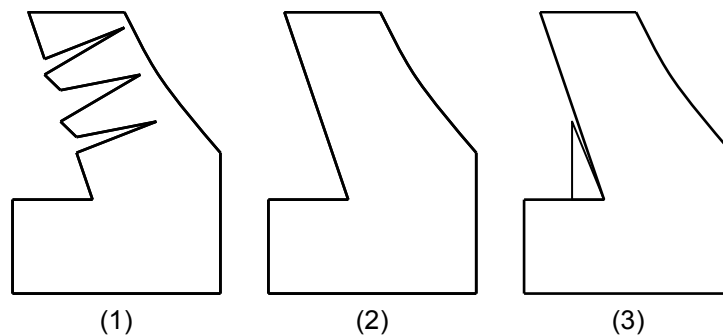
Figure 1 Three basic chip types (1) discontinuous (2) continuous (3) continuous with built-up edge adjacent to tool face.[5]
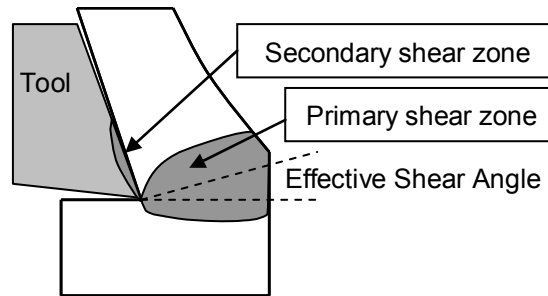
Figure 2 Shear zones and shear plane in continuous chip formation.

Continuous chip formation can approximate a steady-state process. However, discontinuous chip formation never approaches steady-state.[7] Continuous chip formation with build-up also never approaches steady state because the build-up is often erratic and breaks off. These three types of chip formation are not comprehensive descriptions, but sufficient to describe chips from most metals that are not of particularly low thermal conductivity, such as many stainless steels.[7,8] Segmented chips tend to form at high speeds because the drop in yield strength due to heating is greater than the yield increase due to strain hardening.[8]

The chip formation model of Ernst was expanded by M. E. Merchant into a two-dimensional model for metal cutting, called the orthogonal cutting model.[9-11] The orthogonal cutting model assumes the formation of continuous chips. Gray iron machining generally results in highly fractured, non-continuous chips that form in a three-dimensional manner; therefore the orthogonal cutting model is not directly applicable to gray iron machining. Cast irons chips have often been classified as discontinuous. An excellent example of type 1 chips forming from gray iron is given by Cook, et al.[12] In their work Cook, et al. found that chips of ferritic gray iron possessed cracks in the direction of maximum shear stress which indicated plastic fracture. Discussion was provided suggesting chips of gray iron could form with elastic, tensile fracture ahead of the tool tip. This type of chip formation was not described by the work of Ernst. An example of such chips was presented by Marwanga, in his PhD work. He determined that chips formed from gray iron with >99% pearlite do not exactly fit the models of Ernst or Merchant.[13] Instead of forming a plastic deformation region ahead of tools in the three standard chip types, gray irons with either A or D graphite were shown to fracture ahead of the tool (see Figure 3). Other graphite types in gray iron were not studied.

4
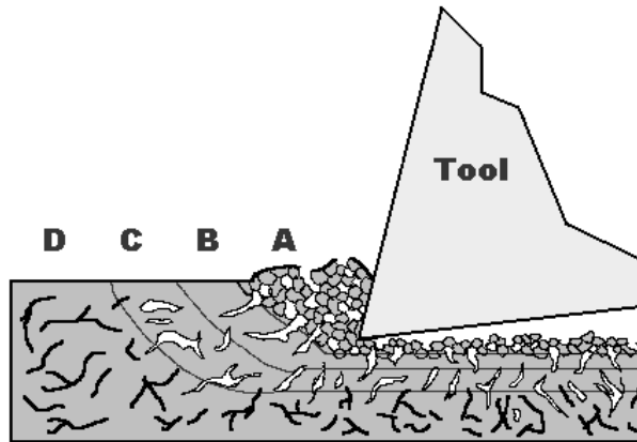
Figure 3 Machining Affected Zone described by Marwanga contained four regions A) shattered zone B) fracture zone C) decohesion zone and D) unaltered material.[13]

Marwanga video recorded chip formation on polished and etched plates during the machining process of shaping at 2 in/min. For comparison of chip formation under industrial machining parameters, a quick-stop-device was used on a lathe when machining bars of gray iron. In both shaping and turning experiments, Marwanga reports there was "very little" plastic deformation at the root of chips. When the same experiments were performed on leaded, free-machining steel, video showed significant material flow and plasticity ahead of the tool rather than the fracture observed when machining the highly pearlitic gray iron. Marwanga concluded that the fracture mechanism of the steel was localized shear deformation until fracture, whereas in gray iron was a mostly elastic strain until fracture occurrences that initiated at graphite flakes. In both gray and ductile irons studied by Marwanga, the chip lengths decreased as spindle speed increased. This decrease could be because the added speed increases the strain rate which in turn decreases ductility.

2.1.2.1.   Consideration of adiabatic shear banding in gray iron chips.

In chip formation adiabatic shearing is brought on by sudden decreases of material flow stress caused by near adiabatic conversion of mechanical work into heat.[14] In a review of literature, Rogers stated a few characteristics of adiabatic shear bands in steel are apparently consistent.[15] Characteristics include the bands etch white, have a fine grain size measured in tenths of micrometers, and have a relatively high hardness. He made no mention of adiabatic shear observations in cast irons. Adiabatic shear and the accompanying phase transformations in the shear bands are not observed in continuous chips when machining steel.[16] Matsumoto, et al. found that when facing AISI 4340, the transition from continuous chips to segmented chips was caused by microscopically visible adiabatic shear band formation.[17] The segmented chips and shear bands did not appear unless the steel hardness was greater than R_C 50 when machining at 91.4 m/min. Recht determines by literature review that during machining of mild steel adiabatic shearing does not appear until the speed reaches 1300 sfpm[18] In machining of gray cast iron for this project neither a spindle speed of 1300 sfpm nor a workpiece hardness of R_C 50 were reached. A conversion from continuous chips to segmented chips like those from adiabatic shearing in steel was also not observed. The

5

difference in conditions required for the appearance of adiabatic shearing in steel and the conditions of machining gray cast iron make it unlikely that gray iron chips have any adiabatic shear bands.

2.1.3. Tool Wear.

Life of the tools used for machining plays a dominant role in machining cost. For this reason most handbooks provide machinability values in terms of tool life.[19] The standard practice for determining the life of the tools is to measure the progression of tool wear under specified conditions. Tool life is typically defined as the time to reach a pre-determined value of tool wear. The costs associated with tool wear and its importance to industry necessitates an understanding of tool wear types and causes.

2.1.3.1. Tool wear types.

There are a variety of tool wear classifications. Of those types, only three need be introduced to provide the background needed in this project: crater wear, flank wear and build-up formation. Figure 4 presents the geometry and related terminology for an indexable tool insert.
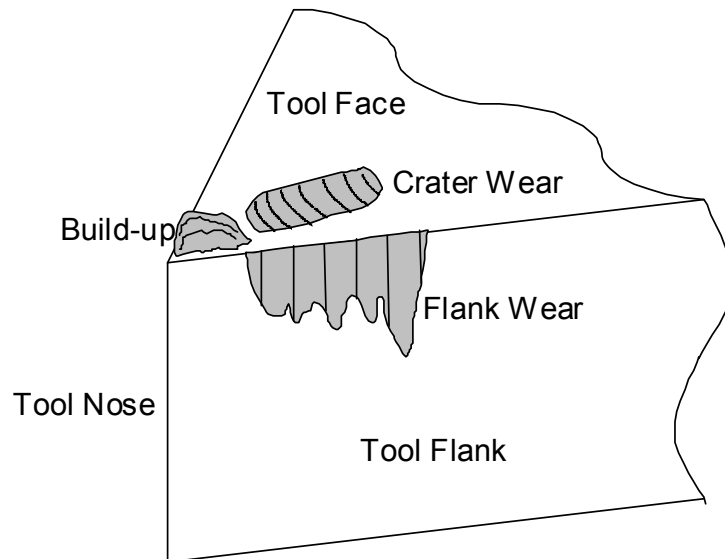
Figure 4 Tip of tool with flank wear, crater wear, and build-up illustrated.

Flank wear is considered to be the most common type of tool wear. Cratering of the tool face occurs in an area away from where the tool face meets the flank. High temperature and pressure present on the tool face during machining can cause welding of the work material to the tool. When this welding occurs it is called build-up edge, or simply, build-up. The causes of these wear types are combinations of abrasion, diffusion, and adhesion.

2.1.3.2. Causes of tool wear.

Wear mechanisms of abrasion, work material adhesion, attrition, tool fatigue, binder diffusion, and tribochemical wear can all contribute to tool wear.[20-22] The flank and crater wear mechanisms of the tools used for research will be abrasion, diffusion, and adhesion.[23]

Abrasion is the dominating cause of flank wear and results from the movement across the tool of hard particles in the work material. With the high pressure of the machining the particles can carry away small portions of the tool with the chips. When cutting cast irons with tungsten-carbide tools abrasive wear is possible from carbides and mold sand, but tungsten-carbide is harder than either of these so the abrasive component to wear is expected to be small.[24]

The temperatures and pressures on the tool flank and face during machining are large enough that atomic diffusion can take place between the work material and tool. Diffusion alone may not be enough to change the shape of tools but can lead to a loss of hardness and strength which increases the susceptibility of tools to abrasion. Diffusion and the abrasion that can follow are often associated with crater wear formation in cubic-boron-nitride (CBN) tools. Huang and Dawson found that when using CBN tools to machine AISI 52100, wear from diffusion was negligible and contributed to less than 1% of the total wear.[20] Narutaki, et al. used experiments in a pressure-controlled furnace to search for diffusion between CBN tools and S55C plain carbon steel (Japanese, 0.55C) determined that the conditions experienced during turning of steel samples were not severe enough for significant diffusion.[25] Diffusion is also believed to cause crater wear in tungsten-carbide cermet tools with cobalt binders (WC-Co) and occurs at temperatures at the tool face ranging from 850-1200°C.[26] Diffusion can also contribute to flank wear of WC-Co tools when machining plain carbon steel at speeds greater than 280 ft/min.[27] Coatings of titanium-carbide, titanium-nitride, or alumina provide significant resistance to diffusion wear in WC-Co tooling.[28]

High temperature and pressure on the tool face sometimes create conditions favorable for welding of work material to the tool. Once this welding occurs the adhered material on the tool is known as build-up. Adhesion of work material to the tool is solely responsible for the observances of build-up, although break-off of the build-up can contribute to other tool wear types and poor surface finish.

Other instances have been found where two or more wear mechanisms have contributed to a single wear phenomenon. Sikdar and Chen reported that, when turning AISI 4340 with TiN/TiC/Al$_2$O$_3$ coated carbide tools, the dominant wear mechanisms were abrasion and adhesion which worked together to generate flank wear.[29]

2.1.4. Tool forces during turning.

Forces acting on the tool during cutting have been applied in tool condition monitoring and in the study of machinability. Tool force data for oblique cutting is collected along three axis directions, each at 90 degrees to the others. Figure 5 provides a diagram relating force data collection axes to the machining operation. The normal force is the response to chip formation and removal. The feed force is the response to the tool moving into the workpiece in the feed direction. The third component, the passive force, is dominated by the response of the tool flank rubbing against the workpiece and sometimes chips pressing against craters or chip breakers.
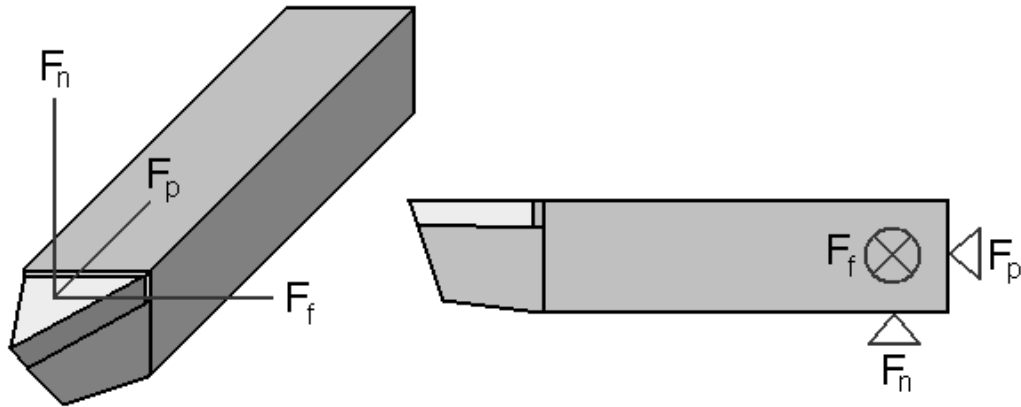
Figure 5 Forces acting on the tool during an oblique turning operation. Normal force has sometimes been referred to as cutting force or tangential force. Passive force has sometimes been referred to as radial force.

In ferrous materials, a linear or near linear increase in cutting force is observed as a function of increasing depths of cut or feedrates.[30] Forces are least affected by changes in cutting speed and any speed changes can increase, decrease, or have no effect on tool forces.[30,31] While performing experiments with turning of steel Chao and Trigger observed that with increasing cutting speed normal and feed forces increased, then decreased, and then started increasing again.[32] For many steel alloys, tool forces increase with increasing hardness. However, there are exceptions to this trend. Results from de Lima, et al. for turning of AISI 4340 steel show that over a hardness range of about 250 to 345 HV (~22 to 35 Rc) the cutting forces decrease.[30] The authors claimed that the decrease evolves from a balance between the higher strength requiring more energy to shear material into chips and increased brittleness of the material providing a higher chip removal rate. Increasing the chip removal rate will reduce the chip-tool contact area and diminish cutting forces. Luo, et al. reported that, for dry turning of AISI 4340 with various hardness values, flank wear on Al_2O_3 and CBN tools decreased with increasing hardness between Rc 40–50.[33] Decreasing tool wear in this hardness region was accompanied by decreases in normal forces with increasing hardness. The decreases in flank wear and normal forces were attributed to reduced fracture energy of the work material in the specific hardness range. Matsumoto, et al. observed decreases in the three tool force components as hardness of AISI 4340 increased while in the range of 30-50 Rc (287-540 HV_{30}). When machining samples of a hardness greater than 50 Rc, forces increased as hardness increased. The authors attributed the change in force behavior to the links between brittleness, heat generation, and workpiece softening. Increasing hardness was said to cause increased tool/chip interface temperature which in turn softened the material just ahead of the tool and lead to reduced chip/tool contact time and forces. Once the steel reached a critical brittleness, the heat generated at the tool/chip contact surface was not enough to significantly soften the workpiece. The decreased temperature was then said to allow for a higher shear force on the rake face.

Observations by various researchers about connections between tool forces and tool wear open possibilities for qualitative or quantitative tool wear estimation in gray cast iron. Sikdar and Chen provide correlations between tool force and flank wear when

machining AISI 4340 with coated carbide tools.[29] They reported the magnitude of all cutting forces increased with increasing flank wear. By analyzing the published tool force data, it was found that a ratio of passive force to feed force consistently increased as flank wear area became larger. The ratio of passive force to normal force consistently increased in two of the three combinations of machining parameters used.

Some research suggests that force ratios, such as the ratio of the passive force to the normal force, are good indicators of tool wear. Smithey, et al. observed in 4130 steel and 80-55-06 ductile iron that for constant conditions, the higher the magnitude of the passive force divided by normal force, the more tool wear was present.[34] The rate of passive force increase as a function of tool wear was not constant, but the rate was constant for the normal force. Lee, et al. applied a neural network and ANOVA statistics to determine that various ratios of forces were better indicators of tool wear than any of the three cutting forces alone.[35]

2.1.5. Energy Use and Distribution During Turning.

Electricity is the source of power for CNC turning. While some electrical energy is consumed by the computer, most of the energy is intended to be spent as mechanical work in the machining process. Efficiencies are associated with the movement of and energy conversions at the spindle and carriage motors. At least 97% of the energy consumed during turning ends up as heat and is dominated by three sources that are shown in Figure 6.[36-38] The largest heat source is the primary shear and deformation zone. The second largest source of heat generation is the region of secondary shear and friction between tool and chip. The smallest heat generation that is still significant is friction between the tool and machined workpiece surface. If energy input required to accomplish shear deformation is reduced then heat generated in this region can also be reduced. A typical distribution of heat is provided in Figure 7.
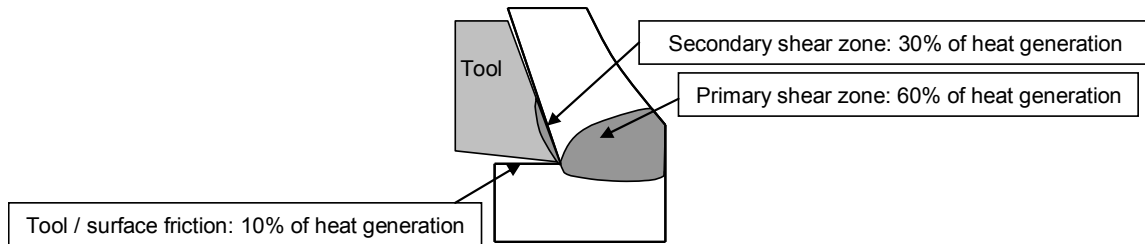
Figure 6 Heat generation sources. Region A is primary shear, region B secondary shear and tool-chip contact friction, and region C tool flank workpiece friction.[37,39]
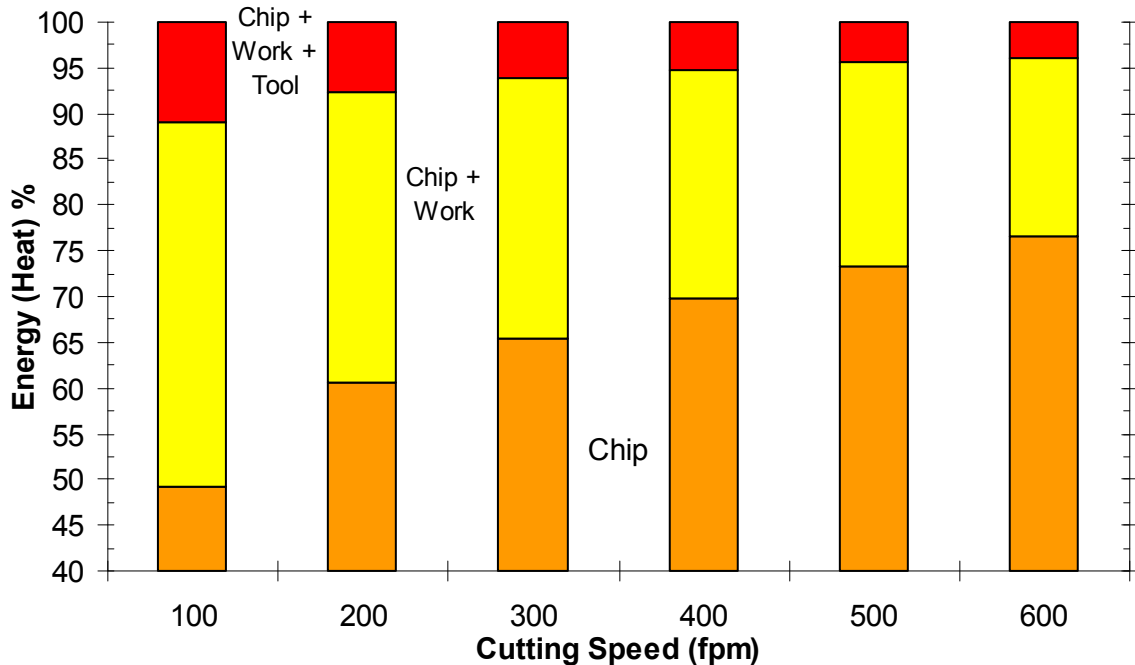
Figure 7 Typical distribution of heat as a function of cutting speed.[40] Data from turning SAE B1113 free-machining steel with K2S with coated carbide tools.

The temperatures of the tool and its interface with chips and the workpiece are considered to be important factors in tool wear formation. Work has been done by many researchers to understand the distribution of heat in and near tools. Figure 8 shows a calculated tool temperature profile. It is important to consider that the temperature values are not likely the same for machining gray cast iron. Indeed, for the experiments presented in this report, the temperatures at the tool/chip interface and in the chip never reach 800°C because at this temperature, diffusion becomes a dominating wear mechanism.[41] As was mentioned when discussing tool wear causes, diffusion should not be a major tool wear mechanism for the machining conditions found in the experiments in this project. Additionally, the conclusion can be drawn that temperatures at the tool/chip interface and in the chip never reach 730°C because, further observation of chips from Peach's showed no signs of matrix phases other than ferrite and pearlite.[44] The machining conditions and the gray irons machined by Peach are considerably similar to the irons machined in this project, providing validity to the comparison.

750-800°C   800-850°C

650-750°C
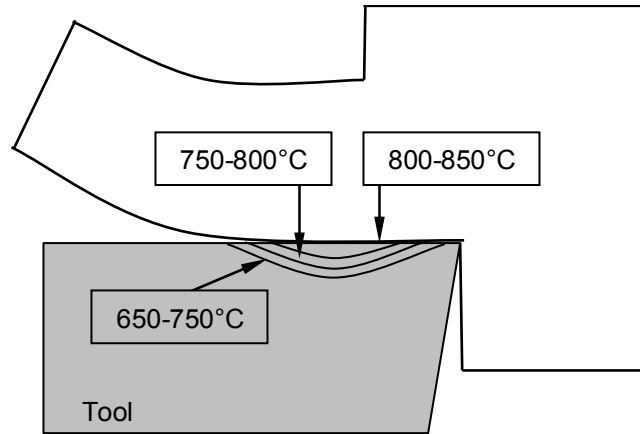
Tool

Figure 8 Tool/chip interface temperature profile from machining low carbon steel at 400 ft/min for thirty seconds.[42]

The force and energy concepts used in turning allow for the estimation of force used to shear the workpiece, calculation of power consumed by the spindle, and a value known as specific cutting energy. Also of interest is the rate at which metal can be machined away from the workpiece by the tool under selected conditions. This rate is called the metal removal rate (MRR) and can be calculated using equation 1,[45] where in equation 1, v = cutting speed in distance per time, f = distance covered in feed direction after one revolution of the spindle, and d = depth of cut.

$$MRR = Vfd \qquad (1)$$

Force acting along the shear plane can be derived using vector algebra and calculated if the normal and passive forces acting on the tool have been measured.[45] Equation 2 can be used for calculation of shear force during chip formation. In equation 2 the variables required are F_n = normal tool force, F_p = passive tool force, and φ represents the shear plane angle. Note that feed force is not used in the calculation and therefore equation 2 assumes an orthogonal cutting condition. Previously, when discussing chip formation, mention was made that machining of gray cast iron does not follow the orthogonal cutting model; therefore, values determined from equation 2 should be considered qualitative and used only for relative comparison.

$$F_s = F_n \cos\varphi - F_p \cos\varphi \qquad (2)$$

The power of the lathe where the spindle holds the workpiece is the power required to perform the machining operation and can be estimated by use of equation 3.[46,47] In equation 3 the variables are defined as, P_s = power at the spindle, F_n = tool normal force, and V = linear cutting speed. Note that because of efficiencies, power at the spindle is less than electrical power input into the spindle motor and to determine the power input to the spindle motor, the power at the spindle needs only to be divided by the efficiency of the motor.[46,47]

$$P_s = F_n V \qquad (3)$$

Specific cutting energy is sometimes calculated as a means of comparing machinability. The value is an estimation energy expended to machine a unit volume of the workpiece.

11

The specific cutting energy (sometimes called the cutting stiffness) can be calculated with equation 4, where Fn = normal tool force, f = feed distance in one revolution, and d = depth of cut.[48]

$$U = \frac{F_n}{fd}$$

(4)

2.1.6. Free Ferrite Skin Effects.

For almost as long as cast iron microstructure evaluation has been available it has been known that the area termed the "casting skin" has a different microstructure than the bulk material, or body, of castings. The casting skin region has no universally accepted definition but is characterized by a different microstructure composition than the bulk of the casting. The casting skin region will often have a variety of type B-E graphite structures instead of the type A structure and can contain free ferrite, pearlite, and carbides. Of particular concern is a predominately ferrite layer with highly undercooled graphite, which is short in length relative to type A. These layers are attributed to short distances for matrix carbon to diffuse to graphite flakes which in turn promotes austenite transformation to the stable ferrite (alpha-iron) phase as opposed to the metastable pearlite phase.[49] An example of a skin layer with free ferrite and highly undercooled graphite can be seen in Figure 9. The effects of the skin layer on tool forces and tool wear needs to be understood if machinability research is performed that includes cutting of the skin. Variables that typically affect gray iron casting skin, such as pouring temperature, inoculation effectiveness, and overall chemical composition, are the same as those that affect overall microstructure.[50,51]

0.015"   0.030"   0.045"
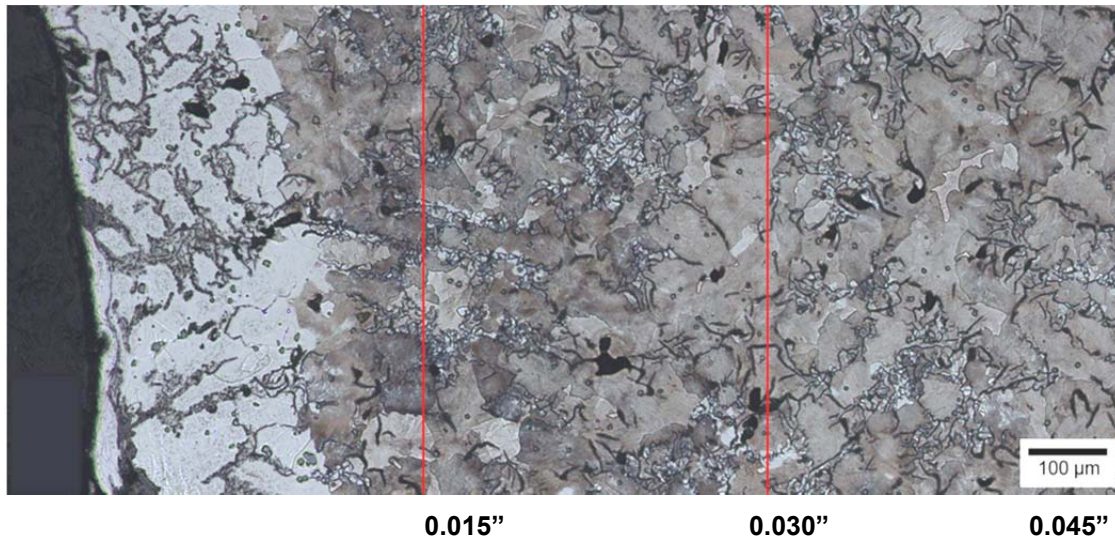
Figure 9 The skin region of a class 40 gray cast iron after etching with 2% nital. The white area is ferrite, the gray is pearlite, and the black is graphite.[43] The graphite flakes become longer on average as the distance from the outermost surface increases.

The effect of free ferrite skin layers on gray cast iron machinability was studied in detail by Peach and various coauthors.[43] Research showed that the combined effects of free ferrite, graphite morphology, and surface geometry significantly changed the machinability of the skin. Cutting forces and specific cutting energy were observed to be

more than double that found when machining the body of castings. It is possible that the increase in forces is a result of the relatively small graphite flakes. With short graphite flakes the skin layer could machine more like ferritic steel than type A graphite cast iron. Support of this was found by Peach when comparing tool forces to graphite flake length.[43] Through surface profiling of the tools used for machining, it was determined that the skin free ferrite also promoted build-up on tool faces. These effects of gray cast iron skin layers on machinability should be considered when analyzing results of gray cast iron machinability studies. Age strengthening may interact differently with the casting skin than with the body of the casting because of the differences in free ferrite and resulting differences in deformation behavior.

2.1.7. Nitride Precipitation in Gray Cast Iron and Iron-Nitrogen Alloys.

2.1.7.1. Aging Effects on Mechanical Properties.

The first published research to suggest the existence of age strengthening (aging) in a cast iron was work done in malleable iron by Kempka in 1955.[52] This study showed that annealed malleable iron demonstrated aging behavior somewhat comparable to that of low-carbon steels. The first published work that found aging in gray cast iron (GCI) was written in 1963 by Ebner, in Germany.[53] Ebner thought pouring had a detrimental influence on tensile strength which he said would decline with storage time, but provided no metallurgical explanation for his thoughts. Publications in 1956[54] and 1969[55] also addressed aging in malleable iron. In 1970, a Russian author published a study of aging in GCI.[56] Nothing further was published on the subject until interest was rekindled with a study in 1999 from Nicola and Richards.[57] Test bars of cupola melted GCI were poured in this study, which was designed to remove the effects of inoculant fade and surface roughness, and the average ultimate tensile strength (UTS) increased by up to 9.9%. Age strengthening has since been observed to increase average UTS of GCI in the range of 3.3% to 13% with corresponding Brinell hardness in the value range of negligible to twenty-three in irons from multiple foundries. Aging has been observed in cupola melted class 30, 35, and 40 gray irons and in class 30, 35, 40, and 45 induction furnace melted gray irons.[57-59] This is not to imply that only these classes of GCI age strengthen, but they are the only GCI with statistically significant results to date. Delaying casting shakeout decreases base GCI strength but does not decrease the percent strength gain from aging.[59] The behavior of GCI's strength and hardness during aging may be seen in Figures 10 and 11, respectively. The same figures also show that regardless of aging, nitrogen increases the strength and hardness of the iron because nitrogen acts to reduce flake length and round the tips of the flakes, an effect linked to higher strength and hardness.[60,61]
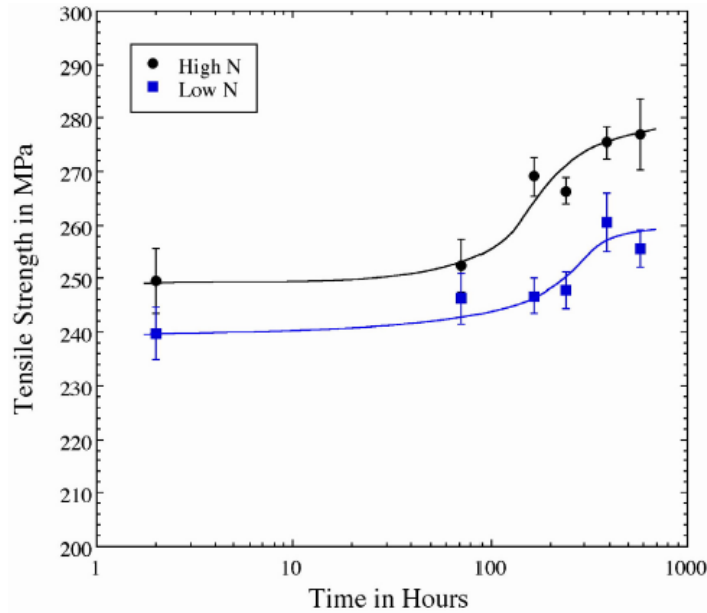
Figure 10 Example of the time-dependant behavior of UTS in age strengthening gray cast iron.[62] Samples are the same as in Figure 11.
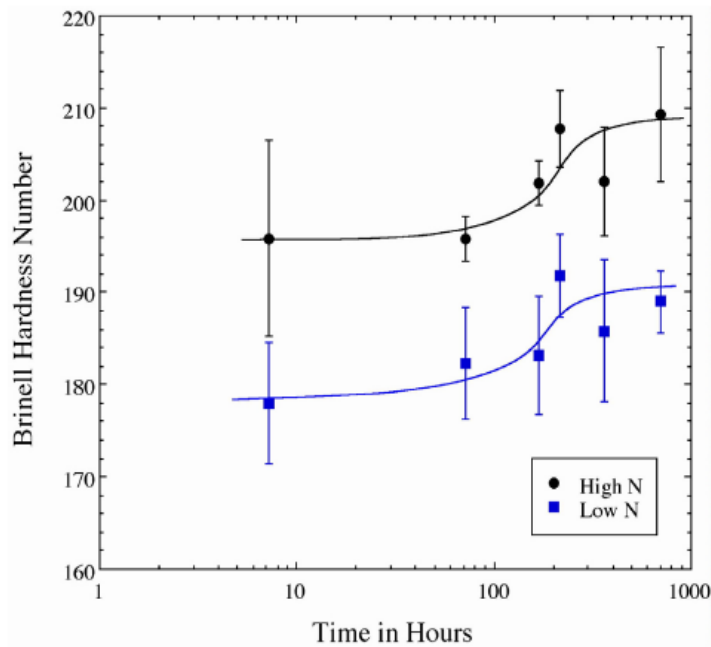
Figure 11 Example of Brinell hardness time-dependant behavior in age strengthening GCI.[62] Samples are the same as in Figure 10.

2.1.7.2. Aging effect on machinability.

Edington, et al. published the first research showing that aging can improve machinability in GCI.[63] His research showed that tilt-rate (deviation of flange perpendicularity), surface finish deterioration rate, and machine power consumption all decrease with aging while tool life increases (see Figure 12). The best surface finish and lowest consumed amperage appeared to be on days three and six of aging. Days

14

of testing before and after this showed improvements over the unaged condition, but were not as good as the day three and day six behavior. Kountanya and Boppana observed similar behavior for tool life improvement with aging.[64] Their results, provided in Figure 13, showed a decrease in tool wear rate with aging that followed a sigmoidal behavior.
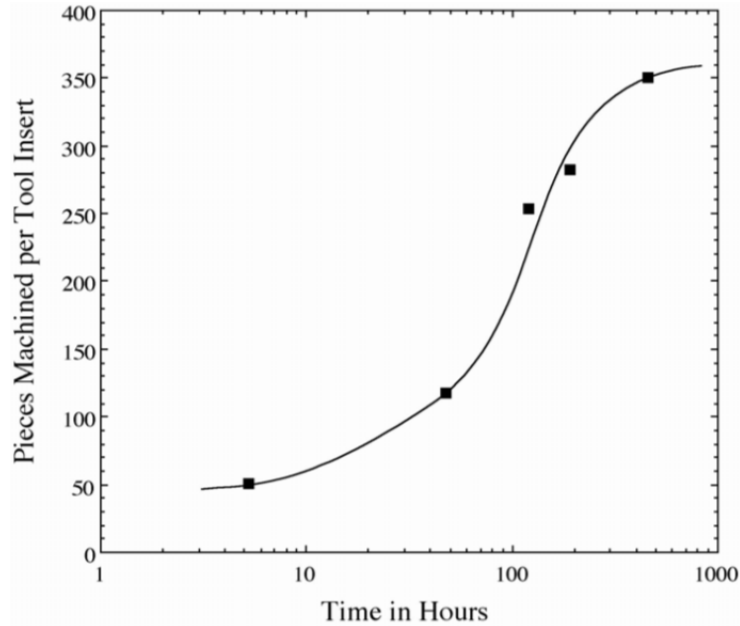
Figure 12 Tool life data for foundry D showed dramatic improvements in the time that the tool was considered to be usable for machining.[65] Tools were Kennametal KY3500 silicon-nitride inserts. It is noteworthy that the improvements in tool life appear to follow the same behavior as the UTS during aging.
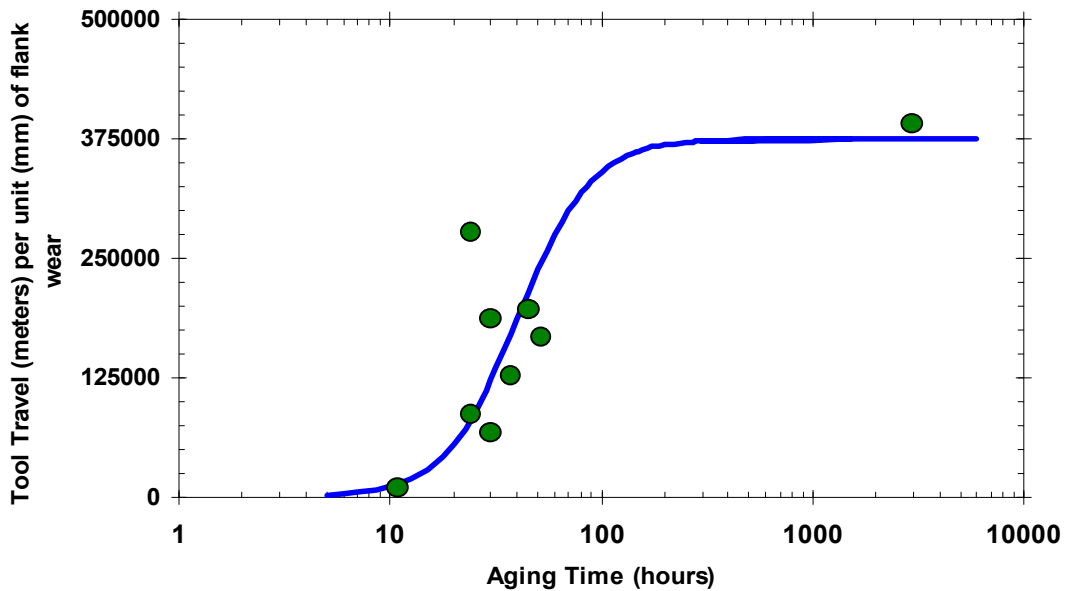
Figure 13 Decrease in tool wear rate observed when machining GCI disk-type castings.[64]

The improvement in machinability accompanied by increases in hardness from aging may be opposite than one would expect in cast iron.[66] It should be noted that, when aging aluminum alloys however, increased hardness can improve machinability.[67]

Determining how machinability changes with aging of cast iron is of practical importance to the iron casting industry so that attempts to optimize machinability can be made.

2.1.7.3.   Consideration of precipitate species.

In the first study by Nicola and Richards, aging appeared to be related to the nitrogen content of the irons studied.[57] Nitrogen is now known to be required to produce aging behavior, and is believed to be consumed as part of precipitate formation.[55-59,63,68] Numerous findings support iron-nitride precipitates as the cause of aging and are discussed, below.

Formation of a nitrogen containing precipitate is possible by a diffusion controlled process because nitrogen has significant diffusivity in iron-based alloys at room temperature.[69] Iron nitride species, such as Fe_4N and $Fe_{16}N_2$, are known to precipitate in some ferrous alloys at room temperature.[70-80] The magnitude of average UTS increase from age strengthening shows an approximate linear fit as a function of nitrogen in excess of stoichiometric titanium.[65] Further support for the notion of an Fe_4N precipitate was found by Richards, et al. by apparent dissolving of the nitrides by heat treatment which allowed nitrogen to be reintegrated into solid solution. A heat treatment at 577°C (1070.6°F) for ten minutes succeeded in removing the strengthening effect of aging.[62] This temperature is below the iron-carbon eutectoid but above the iron-nitrogen eutectoid for Fe_4N. The heat-treated iron was tested immediately after resolutionizing and again after aging at room temperature for thirty days. The strength gain from the first aging returned after resolutionizing and re-aging.

Differential scanning calorimetry (DSC) results appear to show the metastable $Fe_{16}N_2$ nitride transforming to the stable Fe_4N nitride at ~250°C (482°F).[62] The DSC results agree with observations by Enrietto of the presence of various nitrides.[74] Figure 14 shows the DSC results, with appropriate labeling.
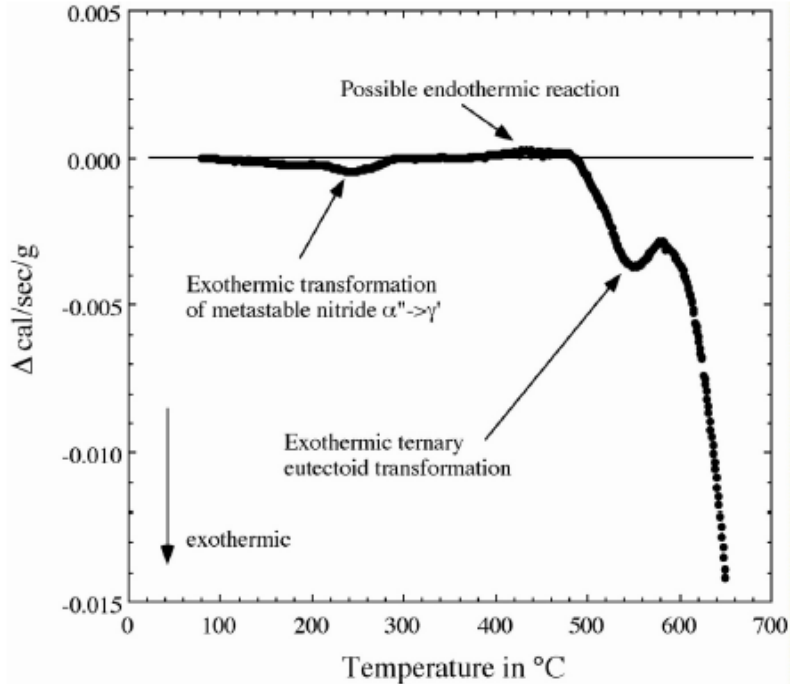
Figure 14 Differential scanning calorimetry showed two exothermic peaks, one of which may represent the formation of the precipitate, Fe$_4$N (γ'), presumed to cause aging.[62] The large exothermic peak is the austenite eutectoid transformation.

Wada and Pehlke determined that chromium increased the solubility of nitrogen in ductile iron without forming a nitride.[81] Other work by Wada, Pehlke, and various co-authors reviewed and/or experimentally determined that chromium increased solubility of nitrogen in both liquid and solid cast irons.[81-84] This increase may or may not have an effect on aging. In practice, nitrogen does not usually reach the solubility limit in cast iron because nitrogen content is controlled by charge materials and nitrogen porosity is not observed in quality castings. Therefore, increasing the solubility limit usually will not actually increase nitrogen concentration in the melt. However, with an increase in the solid solubility limit of nitrogen, decreases in aging could be observed by reducing nitrogen supersaturation of the ferrite near room temperature. No study on chromium or manganese interaction with aging has been conducted in cast irons.

One mechanism briefly considered to explain the age strengthening behavior was titanium-nitrogen substitutional-interstitial clusters interfering with dislocation motion, similar to those observed in steel.[85] Since industrial data have suggested that titanium additions reduce aging or eliminate it altogether, if it is present in sufficient amounts relative to nitrogen, this mechanism is not a candidate to explain aging in cast iron.

Aging tensile bars in an unmachined condition, or aging after machining, has been determined not to affect the magnitude or rate of strength increase.[57] This finding is significant because it rules out a link between hydrogen and aging. Hydrogen diffusivity is so high at room temperature that if aging were caused by diffusion of hydrogen out of the bars, then aging bars in machined condition would significantly increase the rate of aging. This has not been observed. A hydrogen effect is considered further in the discussion with paper reviewers included in research by Nicola and Richards.[59]

In the discussion section of their first paper, Nicola and Richards indicated that, although copper was used to stabilize pearlite, the aging could not be from an ε-copper precipitate like those possible in 17-4PH steel because GCI aging can occur at room temperature.[57] Copper-rich epsilon precipitates require several hundred degrees Celsius to grow since they rely on mobility of substitutional atoms whose room temperature diffusivity is low.

Neutron scattering experiments have been performed on GCI samples previously determined to demonstrate age strengthening. The neutron scattering revealed spherical particle precipitates with diameters ranging from 2nm to 4nm or an ordered array of particles with a spacing of 3.7nm.[64] The neutron scattering results are open to some doubt because inhomogeneities may have been removed from thinner samples; permitting peaks to appear that were not visible in thicker samples. The neutron scattering result has not been linked to a species of precipitate, but may be linked in the future.

A temperature of transition from either a dual or sequential precipitation process to a single precipitation process has been observed in a high-purity Fe-N alloy by Enrietto, who noted a transition to precipitation of only Fe_4N at or above 300°C (572°F).[73] Differences between precipitation transition temperatures could be explained the many elements present in cast iron that were not in Enrietto's high purity alloy because these elements could affect the precipitation kinetics and thermodynamics.

Figure 15 presents two of the most recent representations of the Fe-N binary phase diagram. Authors of Figure 15b indicated that their observation that ferrite and ε-nitride were stable phases at room temperature opposes the previous belief that ferrite and γ'-nitride (Fe_4N) are the stable room temperature phases.[91] The same paper discusses the possibility that although ε-nitride could be the equilibrium phase below about 200°C (392°F), γ' might instead be retained if a temperature near the transformation temperature is not held long enough. The observation of ε-nitride at room temperature agrees with at least one other set of observations by Hrivňák, although these observations have not met the rigors of peer-review.[75,76] A paper by Jack, who extensively studied nitride formation in steel, commented that Fe_3C and Fe_3N are isomorphous and could easily be confused.[92] In light of this, the ε-nitride observed as a stable room temperature by Hrivňák may have been iron-carbon cementite. Notably, Enrietto also observed that dissolution of nitrides took almost as long as their precipitation, which suggests that the nitrogen solubility in ferrite will have the same value in either process.[73] This observation is evidence that Fe_4N is the equilibrium room temperature phase; which supports the phase diagram in Figure 15a as opposed to that in Figure 15b.
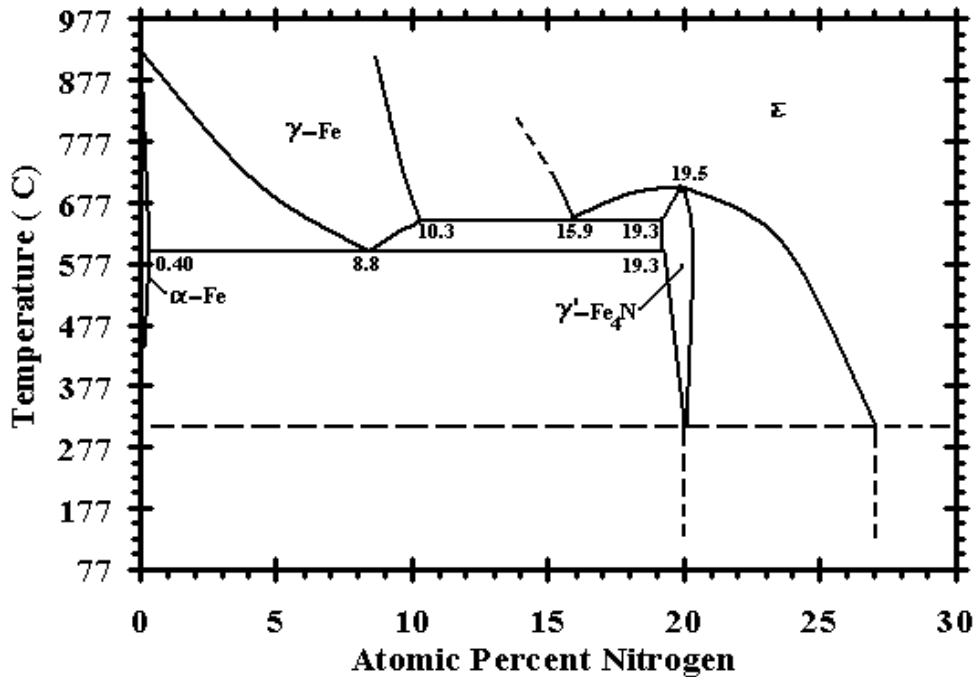
(a)
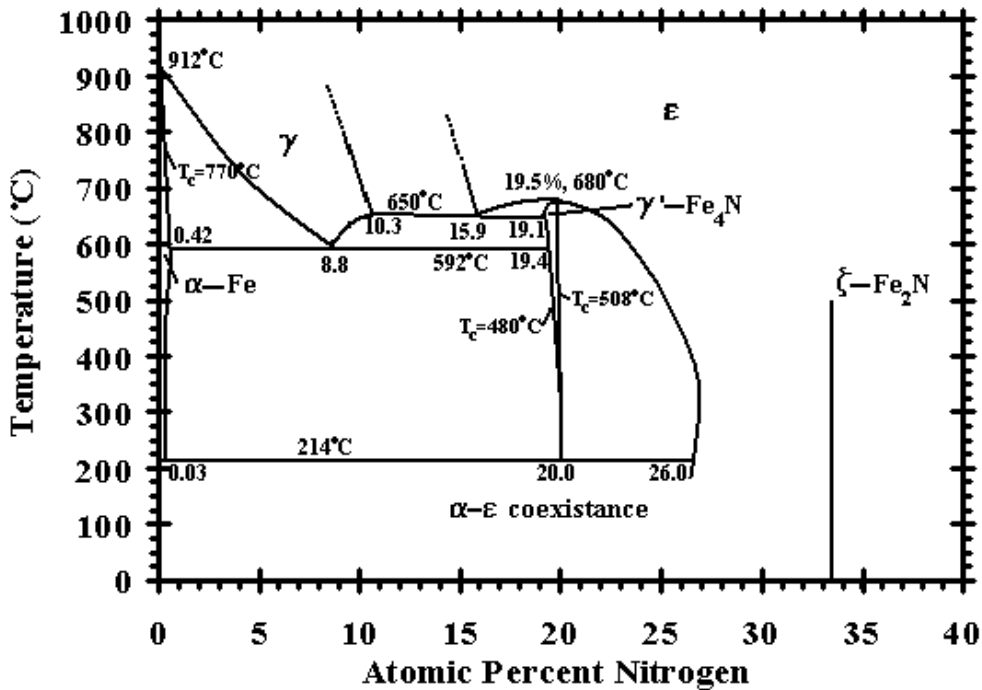
(b)

Figure 15 (a) Phase Diagram proposed by Malinov et al., where ferrite and Fe₄N are equilibrium phases at room temperature.[93] (b) Phase diagram proposed by Du Marchie Van Voorthuysen, et al. in 2002.[91] Phases shown at room temperature are ferrite and ε-nitride.

The phase diagram in Figure 15a, the data and modeling comparisons in Figure 9, and the information presented at the beginning of section 2.1.7.3 are in agreement that the

19

nitride responsible for fully aged behavior in cast irons should be γ'-Fe_4N. To date, the only possible nitride precipitates in cast irons were detected in ferritic malleable cast iron[54] and, indirectly, by neutron scattering.[11] Proof of precipitate species and morphology in cast iron has thus far eluded researchers. To understand the identity and behavior of the precipitates, work completed in less complicated microstructures such as steel and high purity Fe-N alloys can be discussed in context of cast iron. Such work will provide a model for the age strengthening of cast irons until further direct observations can be made.

2.1.7.3.1. Precipitate information inferred from steels.

In a review of precipitation processes in iron alloys, Edmonds and Honeycombe determined that the process for nitride precipitation at high nitrogen supersaturation and temperatures below 200°C (392°F) is: Nitrogen Guinier-Preston (GP) zones $\rightarrow Fe_{16}N_2$ $\rightarrow Fe_4N$.[94] In this case, the precipitation of $Fe_{16}N_2$ from nitrogen GP zones is homogenous. For low nitrogen supersaturation and high aging temperatures the precipitation appears to skip the GP zones and heterogeneously nucleate as $Fe_{16}N_2$. The nitrogen GP zones preceding $Fe_{16}N_2$ formation were observed by M. Wada, et al.[95] Different temperatures have been observed where the direct precipitation of Fe_4N occurs, but the transition temperature can be expected to occur when aging is performed above about 200°C (392°F) or at least above 250°C (482°F).[90] One study by Dahmen, et al. showed that when aging a sample on a high voltage electron microscope stage at 285°C (545°F), $Fe_{16}N_2$ began to precipitate after 1.5 minutes, and Fe_4N began to precipitate and consume $Fe_{16}N_2$ only 2.5 minutes later.[70] Although this technically showed that $Fe_{16}N_2$ can precipitate at temperatures above 250°C (482°F), in practical terms, the process starts with Fe_4N because the $Fe_{16}N_2$ is so short lived.

Dijkstra claimed that Fe_4N was not preceded by any other precipitate, at any temperature.[72] He drew this conclusion despite the observation that other unidentified precipitates formed before Fe_4N and dissolved as Fe_4N grew. Two years later, Jack concluded that the unidentified precipitates preceding Fe_4N formation were a phase, which he named α'' ($Fe_{16}N_2$).[76] One year later, in 1957, Booker, et al.[70] published a paper confirming Jack's discovery of α''-$Fe_{16}N_2$ precipitates and asserting that these were the precipitates observed by Dijkstra[72] and Wert.[96] At least three papers have claimed that the growth of these nitrides in the Fe-N system is diffusion controlled.[71,96,97]

Phillips observed at 45,000X that both $Fe_{16}N_2$ and Fe_4N were present in samples after forty-three months of room temperature aging.[79] This period is much longer than would be expected for the metastable $Fe_{16}N_2$ to be present. Phillips commented that the concentration of solutes other than carbon and nitrogen were not determined and may have prolonged the time the $Fe_{16}N_2$ was present. Jack briefly discussed the possibility that nitriding alloying elements might stabilize $Fe_{16}N_2$ at room temperature.[79]

Precipitates of $Fe_{16}N_2$ have a rosette-type appearance when they are small enough that a transmission electron microscope (TEM) is required for imaging. Some of the better TEM images of precipitates were published by Hale[74] and Phillips.[79] Some of the images by Hale show with clarity that the precipitates were either face-on or edge-on to the direction of observation. Thus, the precipitates appear to be at 90 degrees to one another, indicating possible cubic growth directions relative to the matrix. In a situation

such as extreme supersaturation the precipitates can grow thousands of times larger and become structured as disk precipitates.[78] The $Fe_{16}N_2$ precipitates lie on and are coherent with the ferrite matrix along $\{100\}_\alpha$.[70,74] The Fe_4N precipitates, on the other hand, are only semicoherent with the ferrite in steel and form single-crystal plate-shaped precipitates with their $\{112\}$ planes parallel to the plate faces.[98] The set of twelve habit planes is accepted to be the $\{210\}_\alpha$ family.[98] Thus, the matrix and precipitate have the relationship of $\{112\}\|\{210\}_\alpha$.[70,71,98] The determination of this family as the habit planes for the precipitates is somewhat unusual because the plane is not of dense atomic packing, nor does it contain the matrix close-packed direction. Studies have shown, however, that the atomic arrangements and spacing between the $\{210\}_\alpha$ and $\{112\}_{Fe4N}$ planes are similar when considered in all three dimensions, and all other matches explored would be distinctly different in atomic spacing.[100] The similarity of atomic spacing between $\{210\}_\alpha$ and $\{112\}_{Fe4N}$ planes may explain the choice of habit planes for the nitrides. In 1987, Dahmen et al.[71] claimed that Fe_4N has four variants with habit planes of $\{049\}_\alpha$. This claim has not been refuted or supported in any further literature. In fact, it appears to have been simply ignored. Table 1 summarizes crystallographic data for ferrite and the nitride precipitates.

Table 1 Crystallographic information for ferrite and nitride precipitates in steel that are also suspected to be precipitated in aging cast irons. Information is for room temperature.

Phase	Crystal Structure	Space Group	Lattice Parameter (Å)
α-Fe	BCC	Im3m	a=2.87 [101]
α"-$Fe_{16}N_2$	BCT	I4/mmm [79]	a=5.72 & c=6.29 [79]
γ'-Fe_4N	FCC	Pm3m [79]	a=3.80 [79]

2.1.7.3.2. Precipitation process model.

With the information concerning nitride precipitation in steel, a reasonable model can be proposed for the precipitation in cast irons. Below 200°C (392°F), the following process is likely: $Fe_{16}N_2 \rightarrow Fe_4N$, with the possibly of nitrogen GP zones homogenously nucleating first. It is perhaps difficult to conceive of a homogenous nucleation process in a material as heterogeneous as gray iron, but the presence of the GP zones may be a moot point since such zones have yet to be connected to a physical manifestation during cast iron aging. The reviewed knowledge from steel research and the combination of kinetics and mechanical property measurements in GCI indicate that above about 200°C (392°F) the equilibrium Fe_4N precipitate nucleates directly on dislocations, and there are no intermediate phases. At this time, there is no reason to assume the iron-nitrides in cast iron have a different crystal structure or orientation relative to the ferrite than do the iron-nitrides in steel. The coherency of the precipitates, and thus their interaction with dislocations, may be relevant for understanding of how aging in cast irons is linked to changes in machinability.

3. Results and Discussion

The following section presents the results and discussion of this effort. Specific details can be found in the references cited.

3.1. Cast Iron Natural Aging

The challenge of this work is to complete the understanding of how age strengthening affects machinability so that foundries may be able to utilize the strength improvement by aging and to schedule the optimal operation window for improving casting machinability. The mechanism by which age strengthening changes the machinability of graphitic cast irons is also discussed in this article.

3.1.1. Aging Kinetics

Room-temperature aging phenomena in different types of iron alloys, including cast irons and steels, have been documented in the literature[102,103]. In cast iron with flake graphite, tensile strength increased by 5-15% after 5-30 days of room-temperature aging[102]. Different mechanisms are involved during age strengthening of iron alloys. Edmonds and Honeycombe[96] provided a review of aging studies in quenched *Fe-N* alloys that indicated a three stage precipitation process beginning with the formation of interstitial-atom clusters, followed by nucleation of α''- $Fe_{16}N_2$ and ending with equilibrium α'-Fe_4N. Precipitation of α''-$Fe_{16}N_2$ can be nucleated homogeneously at low temperatures and high nitrogen super-saturations or heterogeneously on dislocations at higher temperatures and low nitrogen super-saturations. In some cases[102], a dip in strength is observed during the start of the aging process.

Elevated temperatures aging kinetics in the cast iron was studied[102,64] based on Johnson Mehl-Avrami and Arrhenius kinetics:

$$V_f = 1 - \exp\left(-(kt)^n\right) \tag{6}$$

$$k = k_0 \exp\left(\frac{-Q}{RT}\right) \tag{7}$$

where: V_f is the fraction transformed, k is the reaction rate constant, n is time exponent, R is the gas constant, T is the absolute temperature, k_0 is an attempt frequency, and Q is the activation energy.

The typical resulting[102] age strengthening curves at different temperatures are shown in Figure 16. An Arrhenius plot was constructed using the rate constants versus the reciprocal of the absolute temperature (Figure 16d). In 182°C – 285°C temperature interval, an activation energy Q was 16.8 kJ/mole and Q increased to 35.7 kJ/mole at below 100°C. The measured value near room temperature was close to the value of activation energy of 44 kJ/mol for precipitation growth of nitrides in *Fe-N* system[104]. Different activation energies at different temperatures are the results of changing aging mechanism. At temperatures above 200°C, the metastable α''- $Fe_{16}N_2$ is replaced by the ordered γ'-Fe_4N. In this regard the neutron scattering studies[7] showed the evidence of interstitial atom clusters that are spherical in shape. The low temperature kinetic results support that conclusion where the time exponent suggests an equiaxially-shaped precipitate.
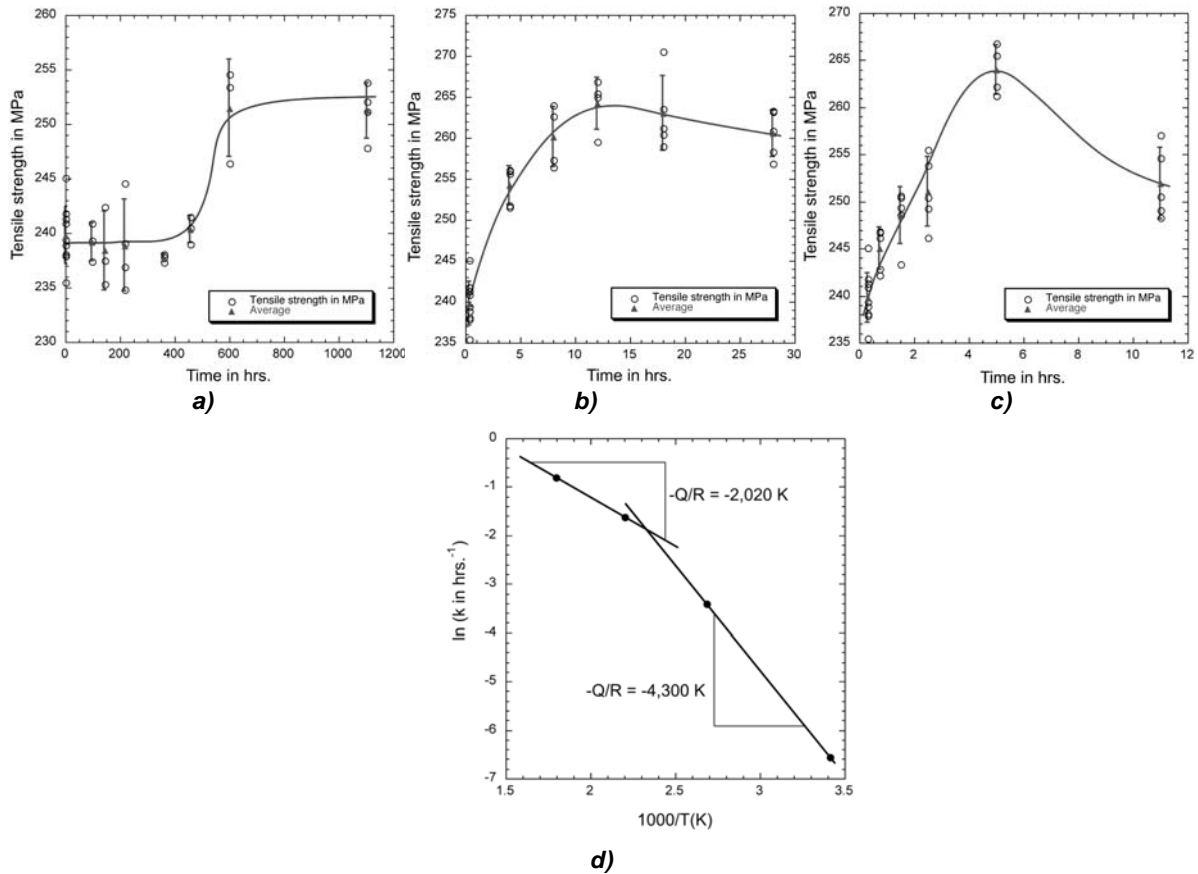
Figure 16 Strengthening of cast iron during aging at room temperature (a), at 182°C (b), and 285°C (c) and Arrhenius plot of cast iron aging kinetics (d)[1].

For practical application, the following relationship between peak aging time (t_{peak}, h) and aging temperature (T, K) was suggested[102]:

$$t_{peak} = 0.171 \exp \frac{2020}{T}$$
(8)

3.1.2. Effect of Alloying Elements

While elevated temperature aging process is less dependent on alloy composition, room temperature aging kinetics is strongly affected by cast iron chemistry. From a practical stand point, the effects of variations in *Mn* and *S* on cast iron aging is important. Table 2 gives a comparison of aging time for two studied cast irons[102,64]. In cast iron with 0.8-0.83%*Mn*, aging was completed at 25 days while this process needed only 15 days for cast iron with 0.51%*Mn*.

Table 2 Comparison of iron chemistry and aging time at room temperature

Parameters	Test[6]	Test[1]
Manganese, wt.%	0.51	0.80-0.83
Nitrogen, wt.%	0.0094	0.007-0.008
Natural aging time, days	15	28

23

To study the effect of alloying elements, aging kinetics of cast irons from six heats with variations in *Mn*, *N*, and *S* was evaluated[106]. Strength change curves typically had a pre-strengthening peak, "relaxation valley" and finally achieved a full age strengthening. Alloying with *Mn* affected on the time for achievement of both pre-strengthening and full strengthening peaks. Cast iron from a heat with 0.53% *Mn* had the highest reaction rate. Iron with lower *Mn* and especially higher *Mn* contents had a longer time of aging reaction.

<p align="center">*a)*   *b)*</p>
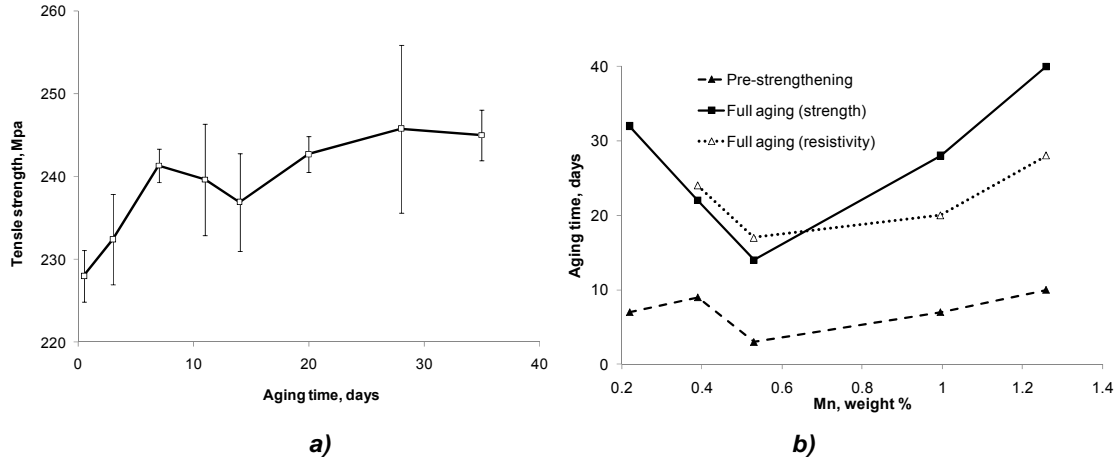
Figure 17 Typical aging curve (a) and effect of Mn on aging time estimated from maximum increase in tensile strength and electrical resistivity (b)[106].

Thermodynamic data and first principle calculations of interaction energy between interstitial *N*-atom and substitutional *Mn* atoms in *Fe-BCC* lattice were used to enhance the understanding of the aging mechanism. The findings suggest the hypothesis that *Mn-Mn* clusters are likely to serve as the nucleation sites for the formation of nitrides in *Fe-Mn-N* system. During this initial period, presumably α''- $Fe_{16}N_2$ precipitates were formed. At the same time, increasing thermodynamic stability of this phase in cast iron with high *Mn* content can delay sequential growth of the stable γ'-Fe_4N responsible for full age strengthening. As a result, a nonlinear effect of *Mn*-alloying on aging kinetics was observed. The effect of manganese on aging kinetics also depends on sulfur concentration because these elements have a strong tendency to *MnS* formation. In this case, the illustrated in Figure 18 full aging time will depend on concentration of free *Mn* (Mn_{free}):

$$Mn_{free} = \%Mn\text{-}1.7\%S \qquad (9).$$
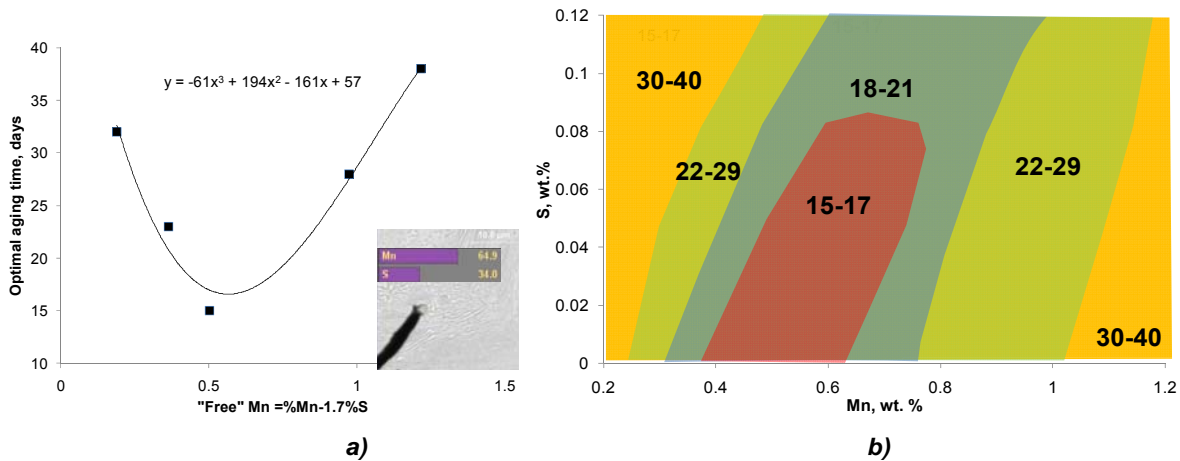
Figure 18 Effect of "free Mn" on full aging time (a) and Mn-S full aging time diagram (b).

3.1.3. Effect of Carbide/Nitride Forming Elements

Cast iron natural aging associates with *Fe-BCC* strengthening by iron nitride precipitation. Such carbide forming elements as chromium promotes decreasing the amount of ferrite in cast iron and reduces the total possible strengthening effect[110]. A representative microstructure from the as-cast machinability test article produced from cast iron with 0.2% *Cr* is given in Figure 19. The metal matrix had a fully pearlitic structure with some white spots identified as the *Cr*-alloyed steadite eutectic ($P\text{-}(Fe_nCr_{1-n})_3C$). This phase has a significantly higher micro-hardness when compared to ferrite or even pearlite and is considered detrimental to machinability. Statistics of tensile test data before and after 21-days of natural aging indicated a detectable by low strengthening.
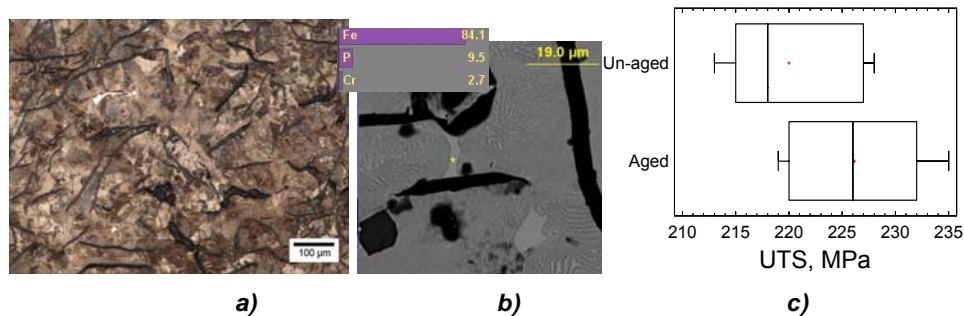
Figure 19 Microstructure of gray iron with 0.2 %Cr (a), SEM/EDS analysis of steadite phase (b), and box and whisker plot of UTS for un-aged/aged conditions[110].

Such nitride forming elements as *Ti*, *Al*, and *B* can even fully suppress iron nitride precipitate strengthening[106,107]. For example, *Ti* had a strong influence on arresting the age strengthening behavior by forming *TiN* and drastically reducing concentration of soluble nitrogen (N_s) in *Fe-BCC*:

$$\%N_s = \%N_{Total} - 0.33\%Ti \tag{10}$$

Figure 20 illustrates the effect of total interstitials N_s in ferrite on the age strengthening in cast iron.

25

Low soluble nitrogen left after *TiN* formation does not allow producing detectible age strengthening of cast iron.

a)

b)
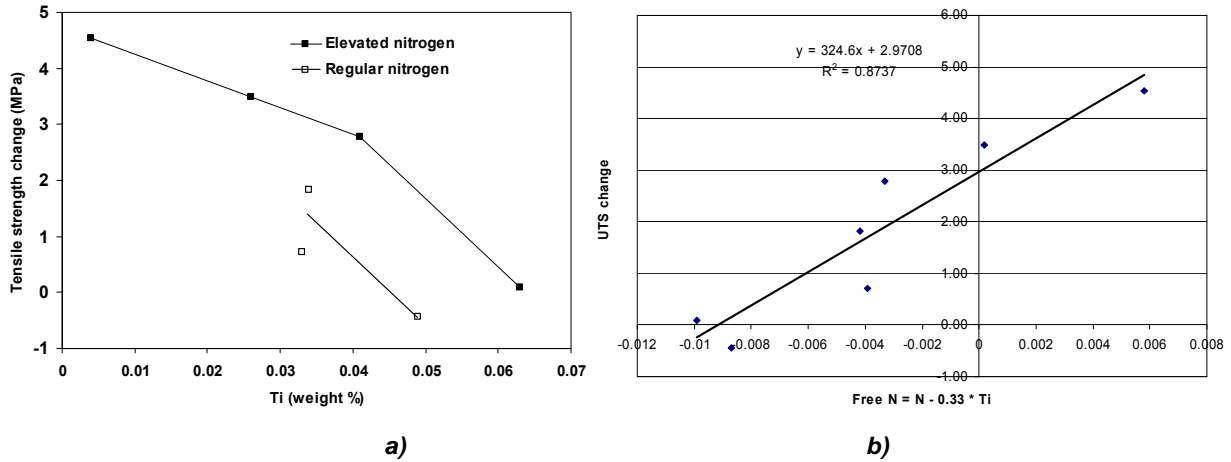
Figure 20 Change in tensile strength with Ti variations at two levels of N (a) and effect of calculated "free" soluble nitrogen on age strengthening[10].

Thermodynamic software FACTSAGE was used[10] for precise calculation of condition when cast iron natural aging will be suppressed by *Ti* impurity (Figure 21). The volume of equilibrium iron nitride significantly depends on the nitrogen content in iron as well as the concentration of nitride-forming elements, in particular titanium, which has a large affinity to nitrogen. When the iron alloy contains titanium and nitrogen simultaneously, these elements react to form titanium nitride resulting in a lower amount of "free" nitrogen in the solid solution. This limits the formation of iron nitride at room temperature and consequently suppresses the iron aging effect. The temperature range of super-saturation of ferrite lies from room temperature to 300°C and beyond this range the possibility of aging is limited according to thermodynamics.

The experimental data[10,11] confirmed these thermo-dynamical predictions. The particular percentage of equilibrium iron nitride is important from a practical point of view because this allows one predicting the age-strengthening effect. The suppressing of natural aging took place when the concentration of titanium exceeded 0.02% in heats with regular nitrogen levels, while in heats with elevated nitrogen, it happened when titanium was higher than 0.06%. Under these conditions, there are no possibilities for iron nitride formation according to the thermo-dynamical predictions. The thermo-dynamic modeling can also be used for more complicated industrial irons containing other impurities which have a potential for reacting with nitrogen.

Low nitrogen (0.004%)

High nitrogen (0.009%)
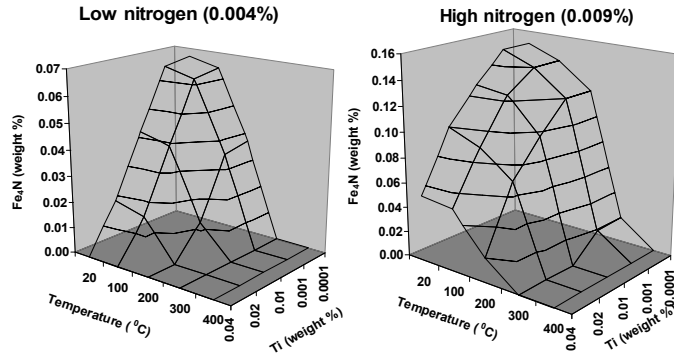
Figure 21 Combined influence of temperature, Ti and N of potential percentage of iron nitrate formation during natural aging[107].

3.2. Machinability of Aged Cast Irons

3.2.1. Cutting Tool Forces

Surface cuts in CNC lathe were performed with using recommended by AFS machinability test article (Figure 22a) produced in laboratory and industrial foundries using green sand molds. Tool force data was collected on a HAAS CNC lathe using a TeLC DKM 2010 Turning Dynamometer[108-109]. Figure 22b shows a schematic of the tool force system, where: F_c is the main cutting force, F_p is the passive force and F_f is the feed force.
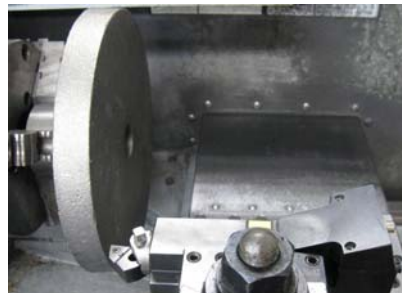
a)
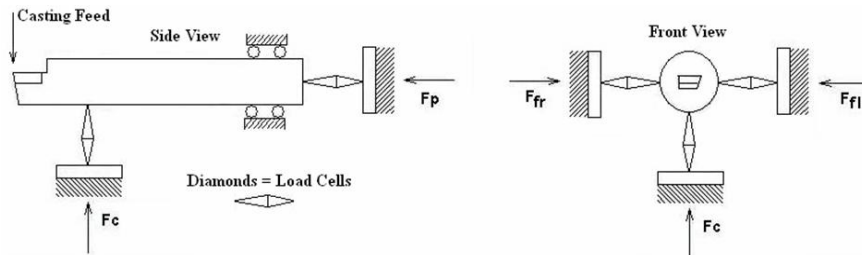
b)

Figure 22 Machinability test of AFS 5J 10" diameter test article (a) and cutting forces measurement system (b).

A series of laboratory tests produced pearlite/ferrite cast irons with variations in carbon equivalent from 3.9% to 4.3% were tested[108] in as-cast conditions and after 25 days of natural aging (Figure 23). In as-cast or un-aged conditions, the cutting forces increased with increasing hardness in irons with different carbon equivalent condition which is

27

typical and predictable. At the same time, there was a reverse type of dependency in which the cutting force decreased with increasing hardness caused only by natural aging in each iron. This unusual behavior could be explained by the energy requirement for chip formation. In un-aged cast iron, soft ferrite absorbs energy for significant plastic deformation. This effect results in edge build-up on the tool tip which could also promote increasing cutting force by enlarging the deformation region (similar to tool wear). In contrast, when iron aging occurs as a result of Fe_4N precipitation in ferrite, it increases the iron's strength and hardness and allows for chip formation with a smaller region of plastic deformation, which could decrease the cutting force. Similar results were achieved also in other cast irons having ferrite in metal matrix and different graphite shapes. For example, aging decreased cutting forces after aging ductile iron with spherical graphite[113].
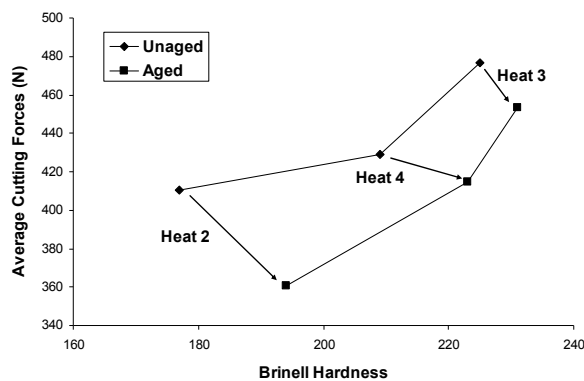
Figure 23 Cutting forces versus hardness for un-aged and aged cast irons[109].

At the same time, aging did not always improve cast iron machinability[110]. For example, aging of cast iron alloyed by carbide forming elements (Figure 19) produced a completely opposite effect on casting machinability (Figure 24). There was a visible and statistically significant increase of the average normal cutting forces of the aged samples compared to un-aged samples. The ratio of passive to normal cutting forces is used as an indicator of tool wear because as a tool loses sharpness it has an increasing passive reaction force. It was visible that this ratio increased more significantly during cutting of aged gray iron.

a)

b)
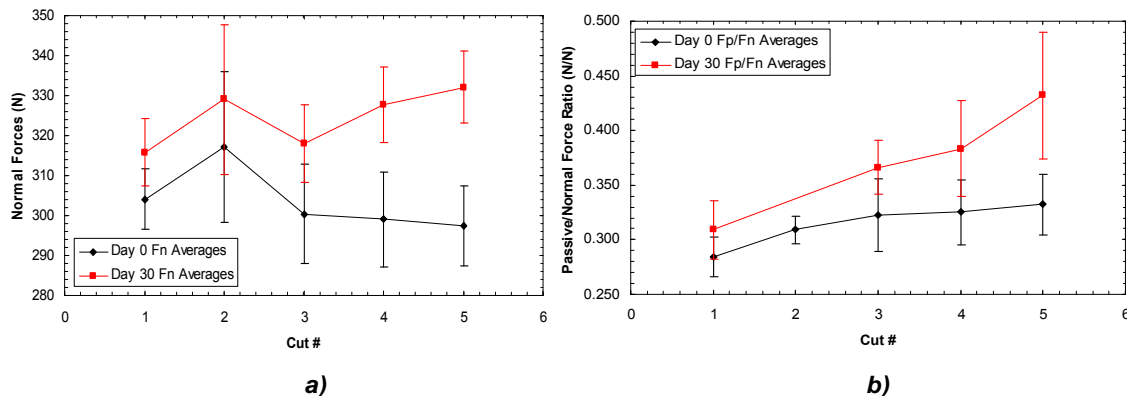
Figure 24 Averaged and standard deviation of normal cutting force (a) and passive to normal cutting force ratio (b) during sequential cuts of high chromium as-cast and aged gray iron[110].

To verify the effect of microstructure on cast iron machinability, castings with the same chemistry were tested additionally after ferritizing/re-solutionizing heat treatment[110,111]. This treatment also produced a re-aging effect and allowed to repeat natural aging. On the contrary to previous test of cast iron with pearlite matrix and steadite phase, aging of ferritized/re-solitionized gray iron improved machinability. The cutting forces were decreased at all studied cutting speeds (Figure 25). It can be concluded from these tests that all gray iron showing improving machinability in aged condition had some amount of free ferrite while gray iron showing increasing cutting forces after aging had no free ferrite and cementite/steadite phases.

a)   *b)*
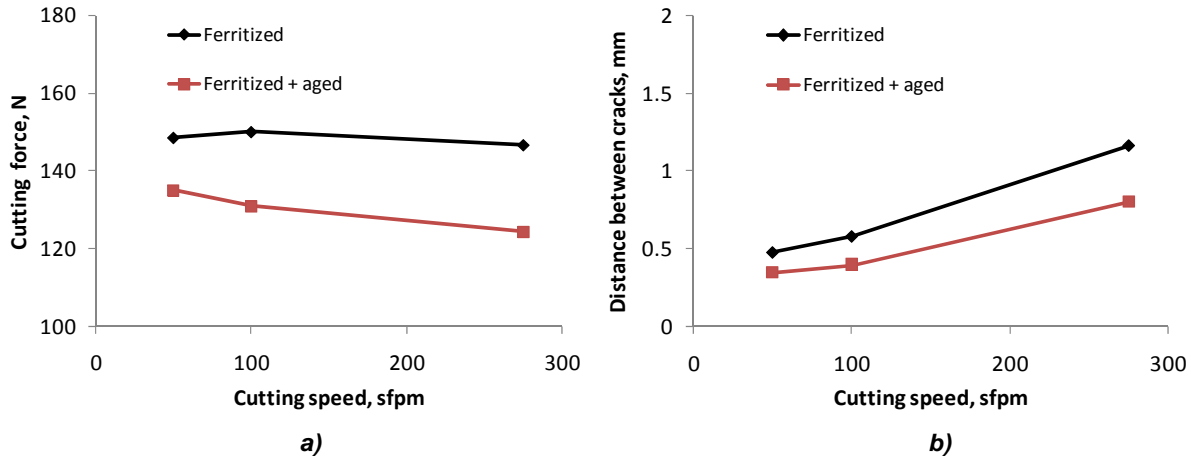
Figure 25 Effects of cutting speed and aging on cuting force of feritized/resolutionized gray iron (a) and effect of cutting speed and aging on an average distance between crack formed in chips[111].

This different behavior of aged cast irons with different types of metal matrix is related to energy of chips formation[110]. Although gray cast iron is a brittle material in tension, chips can experience significant plastic deformation because the stress state during machining is dominated by compression and shear. If chip formation is assumed to be a plastic strain to fracture event, then changes in fracture toughness would logically affect machining behavior. Fracture work during tensile testing was estimated from the stress-displacement curve (Figure 26). In the as-cast condition the work of fracture increased after aging and cutting forces increased at the same time. On the contrary, ferritized iron showed decreased work of fracture due to aging as well as decreased cutting forces[14].

(a)   *(b)*
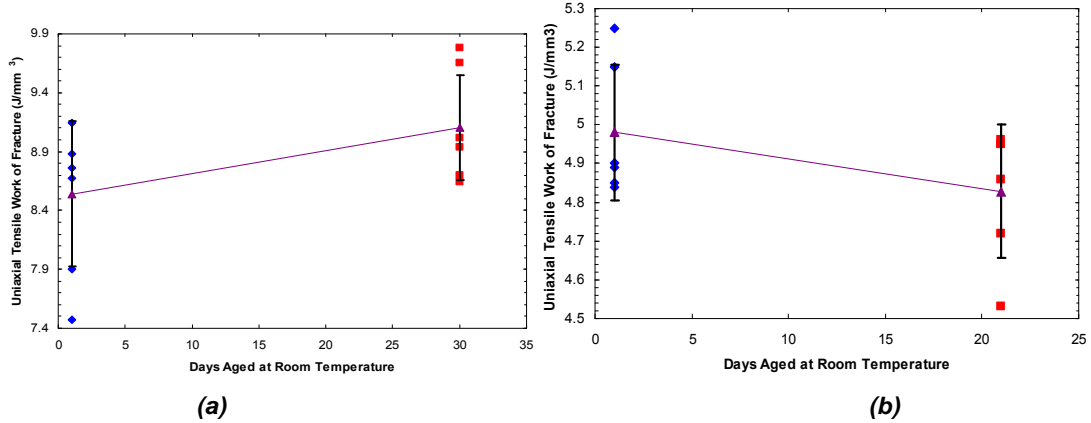
Figure 26 Work of tensile fracture for un-aged and aged gray iron with essentially no free ferrite in the matrix (a) and un-aged and aged annealed gray iron that contained significant free ferrite (b)[111].

3.2.2. Tool Wear and Industrial Machining Parameters

Based on both the current work and that of previous researchers, tool wear is lower when machining gray cast iron aged at room temperature because aged iron requires less work input from the machining center to form and break off chips. The decrease in required work has been demonstrated in the present study[108-110] by tool force measurements and in previous work by testing amperage drawn while machining unaged and aged iron[62]. It was shown that the least power was required to machine castings aged during 3-6 days when compared to 1, 9, and 20 days (Figure 27). At that optimal aging time, machined castings had better surface quality (less roughness).

a)   *b)*
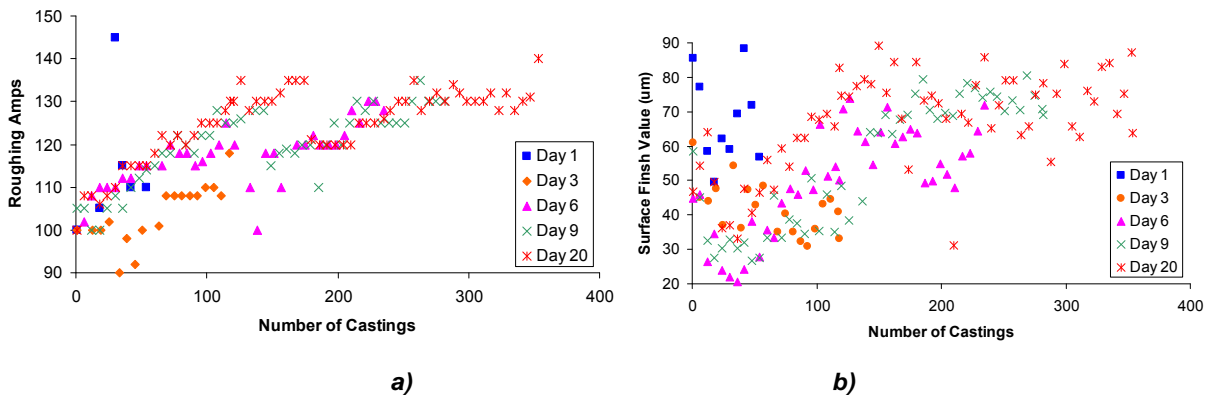
Figure 27 Roughing amperage drawn to machine clutch disks as a function of the number of days the castings were aged and the number of castings machined (a) and surface finish value (b)[62].

Other tests were performed with industrial face machining of brake discs for a passenger car[108,109]. Excessive tool wear produced changing tool geometry and increased cutting forces which promoted elastic deformation of casting with increasing tilt and destroying required tolerance. Tilt data from the machining of industrial castings were compared in two ways. First, Figure 28a compares the tilt during machining of 50 un-aged (Day 1) castings with 50 aged (Day 10) castings. Second, Figure 28b compares the tilt for the same 50 un-aged castings to 200 aged (Day 10) castings. The machining of the 50 un-aged castings required two tool position changes as indicated

by the bold arrows. No tool position changes were required during machining of aged castings after 50 or 200 castings indicating more consistent dimensions and reduced downtime in tool position corrections. Figure 28c gives a comparison of measured tool wear for different operations. Aging significantly decreased tool wear in most of the operations.

a)

b)

c)
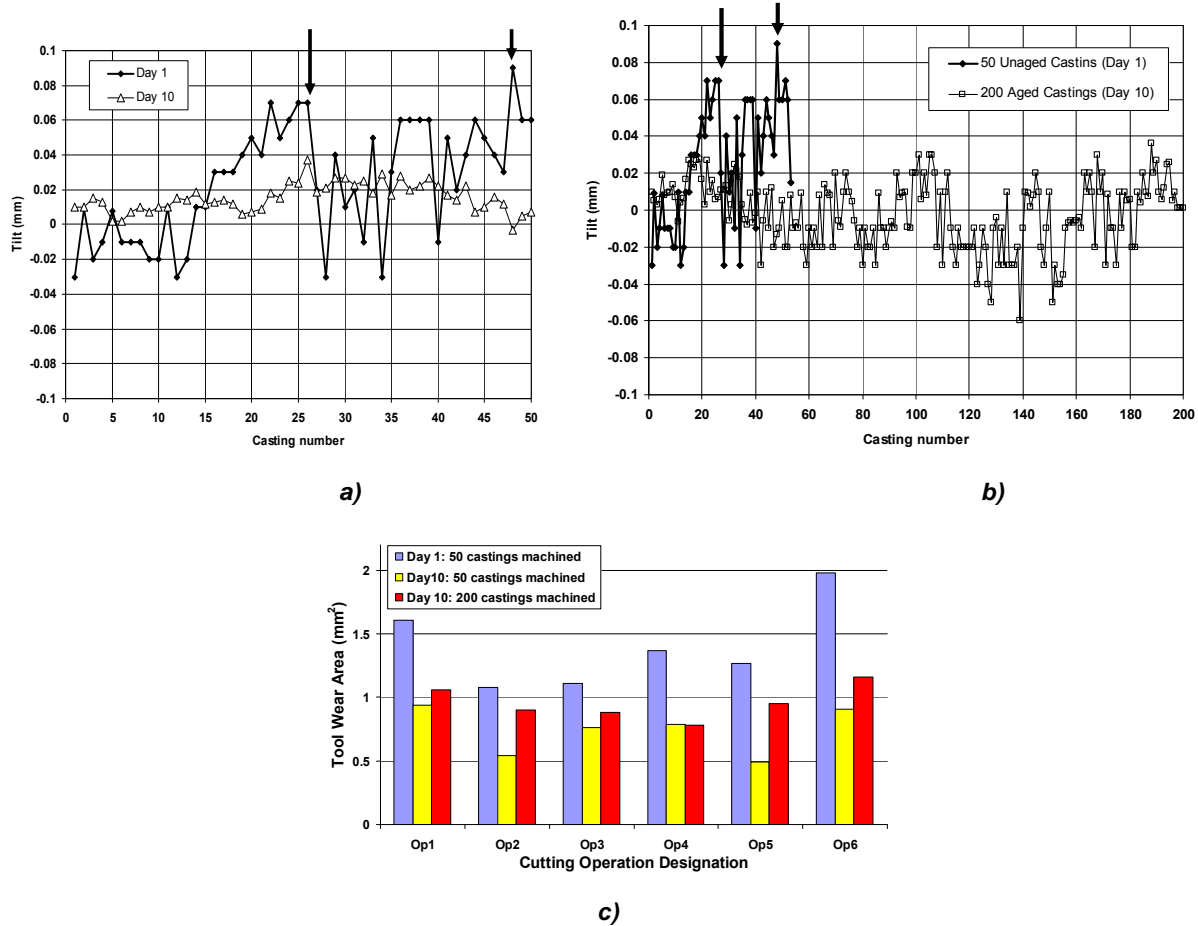
Figure 28 Comparison of tilt data from machining: a) 50 un-aged castings with 50 aged castings and b) 200 aged castings, and c) tools wear (flank area)[108,109].

3.3. Industrial Recommendation for Improving Cast Iron Machinability by Aging

Summarizing the previous and recent experimental studies, it can be concluded that there are three different possible scenarios for changes in machinability of gray iron during natural aging (Table 3).

Table 3 Different aging/machinability scenario observed in gray cast iron [108-111].

Scenario	Gray Iron	Aging effect conformation	Phases, % area		Aging effect on machinability
			Ferrite	Steadite/ carbides	
1	Lab (4.1% CE with *Ti*)	No	5-15	-	Not effected
2	Lab (4.3% CE)	Yes	25-27	-	Improved
	Lab (3.9% CE)	Yes	5-7	-	Improved
	Industrial brake disks	Yes	~1	-	Improved
	Industrial test articles (ferritized)	Yes	40-60	1.8–2.0	Improved
3	Industrial test articles with elevated *Cr* and *P*	Yes	< 0.2	1.8–2.0	Increased tool forces

- *First scenario:* aging does not occur and hence, has no influence on machinability. Lack of aging effects in the iron can be caused by elevated nitride forming elements (particularly *Ti*) relative to nitrogen. Additions of nitrogen to iron are possible and can enhance aging. Thermodynamic data can be applied to determine if there is enough "free nitrogen" for aging a cast iron. Figures 20, 21 and Eq.10 can be used for the prediction of aging effect in a particular iron.

- *Second scenario:* If cast iron has aging, this phenomenon can be used for improving casting machinability. Aging is accompanied by decreasing cutting forces and tool wear. These irons have enough "free" nitrogen to promote age strengthening. Decreased cutting forces and increased mechanical properties were proven in laboratory castings (Figure 23) having different carbon equivalents. These irons had some amounts of free ferrite and no free cementite or steadite. Optimal aging time depends for particular "free *Mn*" content and could be evaluated using Figure 18. Acceleration and decreasing aging time for improving machinability could be done by worm temperature "soaking" (Eq. 8).

- *Third scenario:* Gray iron has elevated concentrations of carbide forming elements such as *Cr* in addition to large *P*. These combinations of chemistry with a particular cooling rate could promote steadite/cementite formation in fully pealitic matrix. This iron had negligible free ferrite in as-cast condition. Aging will increase cutting forces in this iron. Effective inoculation and chemistry control will improve casting machinability by aging in these cast irons.

3.4. Conformation test

Five AFS 5J 10" diameter test articles were poured into no-bake molds from one 200 lbs induction furnace heat. Nitrogen content was enhanced by ladle treatment with 0.2% of *Fe70Mn5N* addition together with 0.3% *Fe75Si2Ba* inoculants. Chemistry and microstructure of mostly pearlitic with approximately 5% ferrite gray iron are shown in Table 4 and Figure 29. Measured hardness in the middle section of the test article was 200-210HB in as cast condition. As cast surface layer (1/8") was preliminary machined

out to avoid the effects of cast surface structure and geometry tolerance on test results. Test articles were face CNC machined at Day 0, Day 5, Day 9, Day 15, and Day 22 with measurement of cutting forces[11-13]. Eight cuts (30 minutes total machining time) were performed from each disc using each time a new tool insert. Thickness of the test article allowed producing duplicated eight cuts and each test was repeated twice. The test results are shown in Figure 30.
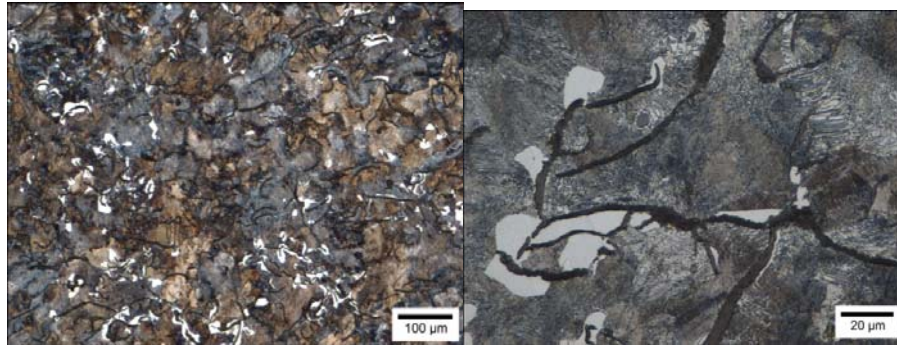
Figure 29 Microstructure of gray iron in machinability article.
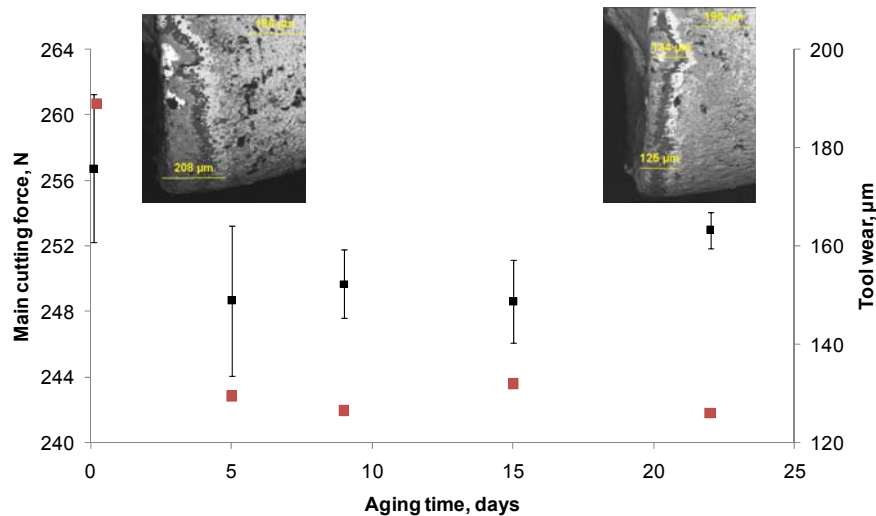
Figure 30 Effect of aging time on cutting force (black markers) and tool wear (red markers).

Table 4 Chemistry (wt. %) of machinability test articles.

C	Si	Mn	S	Cr	Cu	Al	Ti	N
3.26	2.03	0.61	0.08	0.15	0.2	0.01	0.008	0.010

Now, let us to compare these test results with the predictions according suggested methodology:

Step 1- evaluation of the possible age strengthening: N_{free} =N-0.33Ti = 0.01-0.033*0.008= 0.007 wt. % or 70 ppm. According to Figure 21 in gives 0.12-0.14 wt. % Fe_4N and will provide age strengthening (Figure 20).

Step 2 – control microstructure: Figure 29 shows free carbide/steadite matrix with small amount if ferrite around flake graphite. Age strengthening of this type structure can improve casting machinability according second scenario (Table 3).

Step 3. Aging time: according to diagram Figure 18 full aging time is 15-17 days and according to Figure 17 pre-strengthening time is 7-9 days.

These predictions were conformed in the described machinability test. Significant decrease in cutting force and standard variation were observed after 9-15 days of natural aging which is between predicted pre-strengthening and full aging time. Increase aging time to full aging stabilized cutting forces while increased an average value when compared to minimum value. From the other side, tool wear depends not only the average value of cutting force but also the stability of cutting process and tool wear continued to decrease during full aging time.

In summary, based on thermodynamic and first principle atomic calculations, a variety of experimental techniques and industrial studies, the mechanism discussed and aging process kinetics were quantified. More important, the aging process was linked to alloy chemistry and simple rules have been suggested to predict aging and forecast peak age strengthening.

The different scenarios of improving casting machinability by aging were also consisted. Laboratory measured cutting forces and observed during industrial machine tool wear and machining surface quality were linked to aging phenomena. A set of rules was suggested for optimization of process window. Finally, confirmation testing was performed for verification of suggested optimal aging time for improved gray iron machinability.

4. Benefits Assessment

Estimated energy savings in ten years 13.05 trillion BTU, based primarily on yield improvement and size reduction of castings for equivalent service. Also it is estimated that the heavy truck end use of lighter castings for equivalent service requirement will result in a diesel fuel energy savings of 131 trillion BTU in ten years.

ENERGY BENEFITS TABLE					
ENERGY SOURCE	CURRENT TECHNOLOGY BASED ON MS&T AND AFS ESTIMATES (BTU/YR/UNIT)	PROPOSED TECHNOLOGY BASED ON MS&T AND AFS ESTIMATES (BTU/YR/UNIT)	ENERGY SAVINGS (BTU/YR/UNIT)	NO. OF UNITS IN 10 YEARS	CUMULATIVE ENERGY SAVINGS (BTU) Assuming distributed market penetration over 10 yr
	(a)	(b)	(c= a -b)	(d)	(e= c* d)
OIL/GASOLINE/ DIESEL	1.24×10^9 BTU/YR/Foundry	1.22×10^9 BTU/YR/Foundry	1.99×10^7 BTU/yr/foundry	500	7.83×10^{10} BTU
NATURAL GAS	4.43×10^{10} BTU/YR/Foundry	4.36×10^{10} BTU/YR/Foundry	7.12×10^8 BTU/yr/foundry	500	2.81×10^{12} BTU
COAL	6.18×10^{10} BTU/YR/Foundry	6.08×10^{10} BTU/YR/Foundry	9.93×10^8 BTU/yr/foundry	500	3.92×10^{12} BTU
ELECTRICITY +	1.2×10^{11} BTU/YR/Foundry	1.18×10^{11} BTU/YR/Foundry	1.93×10^9 BTU/yr/foundry	500	7.61×10^{12} BTU
OTHER ENERGY	1.24×10^9 BTU/YR/Foundry	1.22×10^9 BTU/YR/Foundry	1.99×10^7 BTU/yr/foundry	500	7.83×10^{10} BTU
TOTAL PER UNIT	20.6×10^{10} BTU/yr	20.268×10^{10} BTU/yr/Foundry	3.31×10^9 BTU/yr/foundry	500	13.057×10^{12} BTU

+ Electricity generation sources need not be shown. Use 10,500 Btu/kWh
+ A unit is defined as an average iron foundry producing 7578T/yr good castings shipped.
Column 1: is the type of energy. Use as many rows as necessary to describe the energy savings applicable to the current technology.
Column 2: (a) is the energy consumed or produced with the current technology.
Column 3: (b) is the energy consumed or produced by the new technology.
Column 4: (c): is the per unit energy savings (derived from 'a - b').
Column 5 (d): is the number of units expected to be in place in 10 years (specify period).
Column 6: (e) is the cumulative savings (derived from 'c * d')
This table should cover all the energy uses, including:
- ENERGY AND PETROLEUM EMBODIED IN THE MANUFACTURE OF PRODUCTS;
- TRANSPORTATION ENERGY FOR HAULING OF WASTE TO DISPOSAL (USE 130,000 BTU/GAL FOR GROUND TRANSPORTATION FUEL);
- ANY COAL OR DERIVED PRODUCT USE;
- ENERGY USED IN WASTE REDEMPTION, TREATMENT OR DISPOSAL;
- ANY PETROLEUM PRODUCT USED;
- ANY NATURAL GAS PRODUCT USED;
- ELECTRICITY (USE A POWER GENERATION RATE OF 10,500 BTU/KILOWATT HOUR)

5. Commercialization

A number of the active foundry/machining co-sponsors implemented the results of the project immediately in their plant operations after plant trials. These include Dalton Foundry, Metals Technology Inc., Rochester Metal Products, Asama Coldwater Manufacturing, Eaton Corporation, and Bremen Foundry.

As a final step, the guidelines for application were published through the American Foundry Society (AFS) to make them available to all foundries which have interest.

6. Accomplishments

Awards

American Foundry Society (AFS) Metalcasting Congress Cast Iron Division Best Paper Awards: 2004, 2005, 2007, 2008, 2009, and 2010.

Publications

"Effect of Alloying Elements on Gray Iron Natural Aging, Part 1: Manganese," S. N. Lekakh, V. L. Richards, J. Medvedeva, J. M. Murphy, Transactions of the American Foundry Society, 119, p 379-388, 2011.

Aging and Machinability of Irons with Compact and Spheroidal Graphite," V. L. Richards, S. N. Lekakh, J. Teague and K. D. Peaslee, AFS Transactions, Vol 118, paper 10-036, p 181-193, 2010.

"Aging Effect on Gray Cast Iron Machinability: Importance of Microstructure," V. L. Richards, J. A. Teague, and S. N. Lekakh, AFS Transactions, Vol 118, paper 10-035, p 195-204, 2010.

"Age Strengthening of Cast Iron: Review of Research and Literature," J. Teague and V. Richards, International Journal of Metalcasting, 4(2), Spring 2010, p 45-58, 2010.

"Age Strengthening and Machinability Interactions in Gray Cast Iron," J.A. Teague, V. L. Richards, S. N. Lekakh, and K. D. Peaslee, AFS Transactions, Vol. 117, paper 09-057, p 475-490, 2009.

"Effects of Nitrogen, Titanium and Aluminum on Gray Cast Iron Microstructure," M.C. McGrath, V. Richards, and T.V. Anish, AFS Transactions, Vol. 117, Paper 09-086, p 497-505, 2009.

"The Effect of Ti and N on Iron Age Strengthening," T. Anish, V. L. Richards and S. N. Lekakh, AFS Transactions, vol 116, paper 08-063, p 653-663, 2008.

"Age Strengthening of Gray Iron – Kinetics Study;" V.L. Richards, T. V. Anish, S.N. Lekakh, D.C. Van Aken, and Wayne Nicola, International Journal of Metalcasting, v10, p 7-18, 2008.

"Aging Effect on Gray Cast Iron Machinability: Tool Force and Tool Wear," J.A. Teague, V.L. Richards, S.N. Lekakh, and K.D. Peaslee, AFS Transaction vol 116, paper 08-134, 2008, p 733-745.

"Age Strengthening of Gray Iron – Kinetics Study" Von L Richards, Thottathil V Anish, Simon Lekakh, David C. Van Aken, and Wayne Nicola, Transactions of the American Foundry Society, vol 115 paper number 07-060, (Each paper is paginated separately in v115 only) 2007.

"Composition Effects on Age Strengthening of Gray Iron", Von L. Richards, Thottathil V. Anish, Simon Lekakh, Wayne, Nicola, and David C. Van Aken, Transactions of the American Foundry Society v114 paper 06-047, p 507-514,2006.

"Effects of Room Temperature Aging on Ductile Iron." <u>Transactions of the American Foundry Society</u>, V. Richards, D. Van Aken, O Mereau, and W. Nicola, v.112.paper 04-038 p 801-811, 2004.

Graduate students thesis

		Degree	Year	Employer
Jared Teague	Dependency of Machinability in Gray Cast Iron on Nitride-Induced Age Strengthening	Ph.D	2010	University of Tennessee, Martin
Thottathil Anish	Age Strengthening of Gray Cast Iron: Alloying Effects and Kinetics Study	MS	2007	Pacific Steel Castings
Olivier Mereau	Room Temperature Aging in Gray and Ductile Cast Iron	MS	2004	Grede Foundries

7. Conclusions

Technical Conclusions:

- Age strengthening was demonstrated to occur in gray iron ductile iron and compacted graphite iron.

- Machinability was demonstrated to be improved by Age strengthening when free ferrite was present in the microstructure, but not in a fully pearlitic microstructure.

- Age strengthening only occurs when there is residual nitrogen in solid solution in the Ferrite, whether the ferrite is free ferrite or the ferrite lamellae within pearlite.

- Age strengthening can be accelerated by Mn at about 0.5% in excess of the Mn/S balance.

8. References

1. E.P. Degarmo, Black, J.T., and Kohser, R.A., *Materials and Processes in Manufacturing,* 9 ed.*;* p. 542. John Wiley & Sons, 2003.

2. M.P. Groover, Fundamentals of Modern Manufacturing : Materials, Processes, and Systems; p. 637. Prentice-Hall, 1996.

3. ISO 3685:1993."Tool-life testing with single-point turning tools"

4. M. Finn, "Putting Iron Machinability to the Test," *Modern Casting,* 30-1 (April 2005).

5. H. Ernst, Knowlton, H. B., Bolton, J. W., D'Arcambal, A. H., Bancroft, W. E., Croft, H. P., *Machining of Metals;* pp. 1-34. American Society of Metals, 1938.

6. M.P. Groover, Fundamentals of Modern Manufacturing : Materials, Processes, and Systems; pp. 556-57. Prentice-Hall, 1996.

7. P.L.B. Oxley, *Mechanics of Machining: An Analytical Approach to Assessing Machinability;* pp. 19-21. Edited by J. M. Alexander. Ellis Horwood Limited, 1989.

8. J.A. Schey, *Introduction to Manufacturing Processes,* 3 ed.*;* p. 627. McGraw Hill, 2000.

9. M.E. Merhcant, "Basic Mechanics of the Metal-Cutting Process," *Journal of Applied Mechanics,* 11 A168-A75 (1944).

10. M.E. Merchant, "Mechanics of the Metal Cutting Process. I. Orthogonal Cutting and a Type 2 Chip," *Journal of Applied Physics,* 16 [5] 267-75 (1945).

11. M.E. Merchant, "Mechanics of the Metal Cutting Process. II. Plasticity Conditions in Orthogonal Cutting," *Journal of Applied Physics,* 16 [6] 318-24 (1945).

12. N.H. Cook, Finnie, I., Shaw, M. C., "Discontinuous Chip Formation," *Transactions of the ASME,* 76 153-62 (1954).

13. R.O. Marwanga, "Quality Improvement Through Microstruture Control for Superior Machinability of Cast Irons"; Doctor of Philosophy in Industrial and Manufacturing Engineering Masters Thesis. Pennsylvania State University, 1998.

14. W.D. Peach, "The Effect of Near-Surface Metallurgy on the Machinability of Cast Iron"; Master of Metallurgy Masters Thesis. Missouri University of Science and Technology, Rolla, 2009.

15. B. von Turkovich, Calvo, S., "Some Applications of Physical Metallurgy in Metal Cutting," *Advances in Machine Tool Design and Research,* 10 pt.2 1051-71 (1969).

16. H.C. Rogers, "Adiabatic Plastic Deformation," *Annual Review of Materials Science,* 9 283-311 (1979).

17. Y. Matsumoto, "Mechanics of Chip Formation and its Effect on the Surface Integrity of Hardened Steels"; PhD Dissertation. Purdue University, 1983.

18. Y. Matsumoto, Barash M. M., and Liu, C. R., "Cutting mechanism during machining of hardened steel," *Materials Science and Technology,* 3 299-305 (1987).

19. R.F. Recht, "Catastrophic Thermoplastic Shear," *Journal of Applied Mechanics,* 31 189-93 (1964).

20. B.H. Amstead, Ostwald, P.F., and Begeman, M.L., *Manufacturing Processes,* 8 ed.*;* p. 466. John Wiley and Sons, 1987.

21. Y. Huang, and Dawson, T.G., "Tool crater wear depth modeling in CBN hard turning," *Wear,* 258 1455-61 (2005).

22. B.H. Amstead, Ostwald, P.F., and Begeman, M.L., *Manufacturing Processes,* 8 ed.*;* p. 468. John Wiley and Sons, 1987.

23. M.P. Groover, Fundamentals of Modern Manufacturing : Materials, Processes, and Systems; p. 571. Prentice-Hall, 1996.

24. Modern Metal Cutting: A Practical Handbook, 1 ed.; pp. II-30. Sandvik, 1996.

25. E.M. Trent, *Metal Cutting,* 3 ed.*;* p. 152. Butterworth-Heinemann Ltd, 1991.

26. N.a.Y. Narutaki, Y., "Tool Wear and Cutting Temperature of CBN Tools in Machining of Hardened Steels," *Annals of the CIRP,* 28 23-8 (1979).

27. E.M. Trent, *Metal Cutting,* 3 ed.*;* pp. 139-42. Butterworth-Heinemann Ltd, 1991.

28. E.M. Trent, *Metal Cutting,* 3 ed.*;* pp. 146-8. Butterworth-Heinemann Ltd, 1991.

29. E.M. Trent, *Metal Cutting,* 3 ed.*;* p. 168. Butterworth-Heinemann Ltd, 1991.

30. J.G. de Lima, R.F. de Ãvila, A.M. Abrão, "Turning of hardened AISI 4340 steel using coated carbide inserts," *ASME Transactions Series B,* 221 1359-66 (2007).

31. P.L.B. Oxley, *Mechanics of Machining: An Analytical Approach to Assessing Machinability;* pp. 76-7, 114. Edited by J. M. Alexander. Ellis Horwood Limited, 1989.

32. B.T. Chao, Trigger, K. J., "Cutting Temperatures and Metal-Cutting Phenomena," *Transactions of the ASME,* 73 777-93 (1951).

33. S.Y. Luo, Liao, Y.S., and Tsai, Y.Y., "Wear characteristics in turning high hardness alloy steel by ceramic and CBN tools," *Materials Processing Technology,* 88 114-21 (1999).

34. D.W. Smithey, S.G. Kapoor, R.E. DeVor, "A new mechanistic model for predicting worn tool cutting forces," *Machining Science and Technology,* 5 [1] 23-42 (2001).

35. J.H. Lee, Kim, D.E., and Lee, S.J., "Statistical analysis of cutting force ratios for flank-wear monitoring," *Materials Processing Technology,* 74 104-14 (1998).

36. B.H. Amstead, Ostwald, P.F., and Begeman, M.L., *Manufacturing Processes,* 8 ed.*;* p. 463. John Wiley and Sons, 1987.

37. M.P. Groover, Fundamentals of Modern Manufacturing : Materials, Processes, and Systems; p. 562. Prentice-Hall, 1996.

38. E.P. Degarmo, Black, J.T., and Kohser, R.A., *Materials and Processes in Manufacturing,* 9 ed.*; p. 510. John Wiley & Sons, 2003.

39. E.P. Degarmo, Black, J.T., and Kohser, R.A., *Materials and Processes in Manufacturing,* 9 ed.*; p. 511. John Wiley & Sons, 2003.

40. E.G. Loewen, Shaw, M. C., "On the Analysis of Cutting-Tool Temperatures," *Transactions of the ASME,* 71 217-31 (1954).

41. P.L.B. Oxley, *Mechanics of Machining: An Analytical Approach to Assessing Machinability;* p. 185. Edited by J. M. Alexander. Ellis Horwood Limited, 1989.

42. E.M. Trent, *Metal Cutting,* 3 ed.*; p. 79. Butterworth-Heinemann Ltd, 1991.

43. M.P. Groover, Fundamentals of Modern Manufacturing : Materials, Processes, and Systems; p. 547. Prentice-Hall, 1996.

44. M.P. Groover, Fundamentals of Modern Manufacturing : Materials, Processes, and Systems; p. 554. Prentice-Hall, 1996.

45. M.P. Groover, Fundamentals of Modern Manufacturing : Materials, Processes, and Systems; p. 558. Prentice-Hall, 1996.

46. B.H. Amstead, Ostwald, P.F., and Begeman, M.L., *Manufacturing Processes,* 8 ed.*; p. 455. John Wiley and Sons, 1987.

47. E.P. Degarmo, Black, J.T., and Kohser, R.A., *Materials and Processes in Manufacturing,* 9 ed.*; p. 494. John Wiley & Sons, 2003.

48. *ASM Handbook Volume 15: Casting* pp.793. ASM International,2008

49. G.S. Narasimha, and Wallace, J. F., "Factors Influenceing the Ferritic Layer on the Surface of Gray Iron Castings," *Transactions of the American Foundry Society,* 531-50 (1975).

50. S. Matijasevic, Gomez-Gallardo, J., and Wallace, J. F., "Ferritic Surface Layers on Gray Iron Castings," *Transactions of the American Foundry Society,* 571-92 (1974).

51. G.E. Kempka, "Embrittlement, Toughening, and Subcritical Thermal Treatment of Malleable Iron," *AFS Transactions,* 63 675-82 (1955).

52. R. Ebner, "Influence of Ageing, Sampling Site and Machining of Test Specimens Upon Tensile Strength and Hardness of Grey Cast Iron," *BCIRA,* 50 689-91 (1963).

53. C.A. Beiser, Evans, E. B., "You Can Quench-Age Malleable Iron," *Modern Casting,* (October 1956).

54. P.B. Burgess, "Age Hardening Ferritic Malleable," *AFS Transactions,* 172-9 (1969).

55. P.V. Novichkov, "Thermocyclic Aging of Cast Iron at 200 - 280 Degrees C," *Liteinoe Proizvodstvo (in Russian),* 31-5 (1970).

56. W.M. Nicola, Richards, V., "Age Strengthening of Gray Cast Iron, Phase I: Statistical Verification," *AFS Transactions,* 749-55 (1999).

57. W.M. Nicola, Richards, V.L., "Age Strengthening of Gray Cast Iron, Phase II: Nitrogen and Metling Method Effects," *AFS Transactions,* 233-7 (2000).

58. W.M. Nicola, Richards, V., "Age Strengthening of Gray Cast Iron, Phase III: Effect of Aging Temperature," *AFS Transactions,* 1085-95 (2001).

59. M. McGrath, Richards, V., Anish, T., "Effects of Nitrogen, Titanium, and Aluminum on Gray Cast Iron Microstructure," *AFS Transactions,* 117 (2009).

60. W. Stets, Lötschert, A., Wolf, G., "Improving the Mechanical Properties of Grey Cast Iron by Alloying with Nitrogen," *Casting Plant and Technology,* 4-25 (January 2009).

61. V.L. Richards, Van Aken, D.C., Nicola, W., "Age Strengthening of Gray Cast Iron: Kinetics, Mechanical Property Effects," *AFS Transactions,* (2003).

62. J. Edington, Nicola, W., Richards, V.L., "Age Strengthening of Gray Cast Iron: Nitrogen Effects and Machinability," *AFS Transactions,* (2002).

63. R.K. Kountanya, Boppana, P., "Optimization of machining of automotive components with polycrystalline cubic boron nitride," *Proc. IMechE Part B: Journal Engineering Manufacture,* 222 797-805 (2008).

64. V. Richards, Nicola, W., "Final Technical Report: Age Strengthening of Gray Cast Iron Phase III," Tri-State University and University of Missouri-Rolla, 2003.

65. C.M. Burke, D.J. Moore, J.R. Parolini, K.B. Rundman, D. Waarala, "Machinability of Gray Cast Iron: A Drilling Study," *American Foundry Society Transactions,* 107 567-75 (1999).

66. A. International, in ASM Handbook, Volume 16, Machining. ASM International, 1997.

69. W.C. Leslie, *The Physical Metallurgy of Steels;* pp. 74-9. CBLS Publisher & Book Distributor, 1981.

70. I. Fall, Genin, J.-M.R., "Mössbauer Spectroscopy Study of the Aging and Tempering of High Nitrogen Quenched Fe-N Alloys: Kinetics of Formation and Fe16N2 Nitride by Interstitual Ordering in Martensite," *Metallurgical and Materials Transactions A,* 27A (1996).

71. G.R. Booker, Sutton, A. L., Phil, D., "An Investigation of Nitride Precipitates in Pure Iron and Mild Steels," *Journal of the Iron and Steel Institute,* 205-15 (1957).

72. U. Dahmen, Ferguson, P., Westmacott, K. H., "A TEM Study of α''-Fe16N2 and γ'-Fe4N Precipitation in Iron-Nitrogen," *Acta Metallurgica,* 35 [5] 1037-46 (1987).

73. L.J. Dijkstra, "Precipitation Phenomena in the Solid Solutions of Nitrogen and Carbon in Alpha Iron below the Eutectoid Temperature," *Transactions Met. Society of AIME,* 185 252-60 (1949).

74. J.F. Enrietto, "The Solubility and Precipitation of Nitrides in Alpha-Iron Containing Manganese," *Transactions of the Metallurgical Society of AIME,* 224 43-8 (1962).

75. K.F. Hale, McLean, D., "Structure of Quench-Aged Iron-Carbon and Iron-Nitrogen Alloys," *Journal of the Iron and Steel Institute of London,* 201 337-52 (1963).

76. I. Hrivňák, "Low-Temperature Ageing of Iron and Low Carbon Steel," *Metal Treatment and Drop Forging,* 175-81 (May 1961).

77. I. Hrivňák, "Low-Temperature Ageing of Iron and Low Carbon Steel," *Metal Treatment and Drop Forging,* 233-42 (June 1961).

78. K.H. Jack, "Binary and Ternary Interstitual Alloys I. The Iron-Nitrogen System: The Structures of Fe4N and Fe2N," *Proceedings of the Royal Society of London Series A, Mathematical and Physical Sciences,* 195 [1040] 34-40 (1948).

79. K.H. Jack, "The Occurrence and the Crystal Structure of α''-iron Nitride; A New Type of Interstitial Alloy Formed During Tempering of Nitrogen-Martensite," *Proceedings of the Royal Society of London Series A, Mathematical and Physical Sciences,* 208 [1093] 216-24 (1951).

80. V.A. Phillips, "An Electron Microscope Study of Quench-Aging and Strain-Aging in A Dilute Fe-C-N Alloy," *Transactions of the ASM,* 56 600-17 (1963).

82. H. Wada, Pehlke, R., "Nitride Formation in Solid Cast Irons," *AFS Transactions,* 81 482-90 (1973).

83. H. Wada, Pehlke, R., "Nitrogen Solution and Titanium Nitride Precipitation in Liquid Fe-Cr-Ni Alloys," *Metallurgical Transactions B,* 8B 443-50 (1977).

84. H. Wada, Pehlke, R., "Nitrogen Solubility and Nitride Formation in Austenitic Fe-Ti Alloys," *Metallurgical Transactions B,* 16B 815-22 (1985).

85. F.N. Mazandarary, Wada, H., Pehlke, R. D., "The Solution of Nitrogen in Solid Cast Irons," *AFS Transactions,* 79 584-8 (1971).

86. W.C. Leslie, *The Physical Metallurgy of Steels;* pp. 137-8. CBLS Publisher & Book Distributor, 1981.

87. W.C. Leslie, *The Physical Metallurgy of Steels;* p. 120. CBLS Publisher & Book Distributor, 1981.

88. W.C. Leslie, *The Physical Metallurgy of Steels;* p. 90. CBLS Publisher & Book Distributor, 1981.

89. C. Wert, "Precipitation Out of Dual Solid Solutions of Carbon and Nitrogen in Alpha-Iron," *Acta Metallurgica,* 2 361-7 (1954).

90. L.J. Dijkstra, Sladek, R.J., "Effect of Alloying Elements on the Behavior of Nitrogen in Alpha Iron," *Transactions Met. Society of AIME,* 197 69-72 (1953).

91. D.A. Porter, Easterling, K.E., *Phase Transformations in Metals and Alloys,* 2 ed.*;* p. 306. CRC Press, 2004.

92. R.E. Reed-Hill, Abbaschian, R. , *Physical Metallurgy Principles,* 3 ed.*;* p. 533. PWS Publishing Company, 1994.

93. E.H. Du Marchie Van Voorthuysen, Chechenin, N.C., Boerma, D.O., "Low-Temperature Extension of the Lehrer Diagram and the Iron-Nitrogen Phase Diagram," *Metallurgical and Materials Transactions A,* 33A 2593-8 (2002).

94. K.H. Jack, "Results of Further X-ray Structural Investigations of the Iron-Carbon and Iron-Nitrogen Systems and of Related Interstitial Alloys," *Acta Crystallographica,* 3 392-4 (1950).

95. S. Malinov, Bottger,A.J., Mittemeijer, E.J., Pekelharing, M.I., Somers, M.A.J., "Phase Transformations and Phase Equilibria in the Fe-N System at Temperatures Below 573 K," *Metallurgical and Materials Transactions A,* 32A 59-73 (2001).

96. D.V. Edmonds, Honeycombe, R. W. K., in Precipitation Processes in Solids (K. C. Russell, Aaronson, H.I., ed.). Met Society of AIME, 1978.

97. M. Wada, Fujii, A., Komazaki, T., Mori, T., "FIM Observation of Nitrogen GP Zones in Iron," *Acta Metallurgica,* 37 2349-55 (1989).

98. C. Wert, "Precipitation from Solid Solutions of C and N in α-iron," *Journal of Applied Physics,* 20 943-9 (1949).

99. E.J. Mittemeijer, Vogels, A. B. P., van der Schaaf, P. J., "Aging at Room Temperature of Nitrided α-Iron," 14 [4] 411-6 (1980).

100. R.F. Mehl, Barrett, H. S.Jerabek, H.S., "Studies Upon the Widmanstätten Structure, VI - Iron-rich Alloys of Iron and Nitrogen and of Iron and Phosphorus," *Transactions Met. Society of AIME,* 113 (1934).

101. L. Cheng, Bouger, A, de Keijser, Th. H., Mittemeyer, E.J., "Lattice Parameters of Iron-Carbon and Iron-Nitrogen Martensites and Austenites," *Scipta Metallurgica et Materialia,* 24 509-14 (1990)

102. Richards, V., Anish, T.V., Lekakh, S., Van Aken, D.C. and Nicola, W., "Age Strengthening of Gray Iron - Kinetics Study", AFS Transactions, Volume 116 (2008).

103. Mililitsky, M., et al, "Room-Temperature Aging of Manganese-Alloyed Nigh Nitrogen Duplex Stainless Steels", *Metallurgical and Material Transactions A*, v. 37A, pp. 2117 - 2123 (2006).

104. Rasek, J., "Activation energies of nitrogen diffusion, nitrides precipitation and resolution in alpha -iron-nitrogen", *Diffusion and Defect Monograph Series*, 7, pp 442 (1983).

105. Edington, J, Nicola, W. M. and Richards, V., "Age Strengthening of Gray Cast Iron, Nitrogen Effects and Machinability", *AFS Transactions*, Volume 110, pp 983-993 (2002).

106. Lekakh, S. N., Richards, V. L., Medvedeva, J., and. Murphy, J. M, "Effect of Alloying Elements on Gray Iron Natural Aging. Part 1", *AFS Transactions*, Volume 119 (2011).

107. Richards, V., Thottathil, V. Anish, Lekakh, S. and Van Aken, David C, "Composition Effects on Age Strengthening of Gray Iron" AFS Transactions, Volume 114 (2006).

108. Thottathil, A, Lekakh, S., and Richards, V., "The Effect of Ti and N on Iron Age Strengthening", *AFS Transactions*, Volume 116 (2008).

109. Teague, J.A., Richards, V.L., Lekakh, S.N., and Peaslee K.D., "Age Strengthening and Machinability Interactions in Gray Cast Iron", *AFS Transactions*, Volume 117 (2009).

110. Teague, J.A., Richards, V.L., Lekakh, S. N., and Peaslee K. D., "Aging Effect on Gray Cast Iron Machinability: Tool Force and Tool Wear", *AFS Transactions*, Volume 116 (2008).

111. Richards, V.L., Teague, J.A., and Lekakh, S.L., "Aging Effect on Gray Cast Iron Machinability: Importance of Microstructure", *AFS Transactions*, Volume 117

112. Peach, W.D., Lekakh, S.N., Richards, V.L., Peaslee K.D., and J.A. Teague, "Effects of Near-Surface Metallurgy on Machinability of Gray Cast Iron," *AFS Transactions*, Volume 115 (2007).

113. Lekakh, S., Richards, V., Teague, J., Peaslee, K., "Aging and Machinability of Irons with Compact and Spherical Graphite," AFS Transactions, Volume, 118, (2010).